In response to the comments made by the reviewers, we have modified our manuscript substantially. The most important comments concern the evaluation of the simulated early Eocene climate and vegetation cover and our hypothesis that vegetation in Central Asia triggers the multi-stability in the Eocene climate. As stated in the reply to both reviewers, we focus on the intransitivity of the climate-vegetation system in a warm, ice-free climate in comparison with the intransitivity in an interglacial climate. In this context, we have chosen the early Eocene as a proxy for a warm, ice-free climate. We did not aim at a best representation of the early Eocene climate.

To emphasize that our study addresses the general understanding of the principles of climate-vegetation interaction, we would suggest changing the title of our study, if this is possible at this stage and if you would agree. In the light of the comments, we find the following title more appropriate to reflect the content of our study: Transitivity of the climate-vegetation system in a warm ice-free climate.

To demonstrate that our simulated early Eocene climate is not completely unrealistic, we added an evaluation of our simulations against reconstructions of zonally averaged early Eocene temperature and reconstructed early Eocene vegetation pattern. This evaluation demonstrates that our simulation by and large agrees with reconstructions.

Following the comment by Referee #2, we performed two additional simulations to test whether vegetation in Central Asia triggers the global multiple vegetation-atmosphere states in the Eocene climate. In the first simulation, we fix the vegetation cover to a desert in Central Asia and to forests elsewhere. After 400 years with fixed a vegetation cover, we let the vegetation evolve dynamically. Analogously, we prescribe a dense forest in Central Asia and deserts elsewhere in the second simulation. Again, the vegetation cover is fixed in the first 400 years and evolves dynamically afterwards.

The additional simulations disprove our old hypothesis. Starting our simulation with forest in Central Asia and deserts elsewhere leads to nearly the same result as found in our simulation that starts from completely barren continents. Likewise, starting from a desert in Central Asia and forests elsewhere leads to the same result as in the simulation starting from completely forested continents. This result motivated a new analysis to find the mechanism that triggers the multi-stability in the warm climate. The outcome of this analysis changes our major findings.

We hope we have addressed all concerns raised by the reviewers.

We thank the reviewers and you, the editor, for your effort.

Sincerely yours,

Ulrike Port and Martin Claussen

1
Manuscript prepared for J. Name
with version 2014/09/16 7.15 Copernicus papers of the LaTeX class copernicus.cls.
Date: 23 October 2015

Stability of the Vegetation-Atmosphere System in the Early Eocene Climate

Ulrike Port[1] and Martin Claussen[1,2]

[1]Max Planck Institute for Meteorology, Hamburg D-20146, Germany
[2]Meteorological Institute, University of Hamburg, Hamburg D-20146, Germany

Correspondence to: ulrike.port@mpimet.mpg.de

Abstract.

So far, the transitivity of the global system has been analysed for late Quaternary (glacial, interglacial and present-day) climate. Here, we extend this analysis to a warm, almost ice-free climate with a different configuration of continents. We use the Earth system model of the Max Planck Institute for Meteorology to analyse the stability of the climate system under early Eocene and pre-industrial conditions, respectively. We initialise the simulations by prescribing either dense forests or bare deserts on all continents. Starting with desert continents, an extended desert remains in Central Asia in the early Eocene climate. Starting with dense forest coverage, the Asian desert is much smaller, while coastal deserts develop in the Americas which appear to be larger than in the simulations with initially bare continents. These differences can be attributed to differences in the large-scale tropical circulation. With initially forested continents, a stronger dipole in the 200 hPa velocity potential develops than in the simulation with initially bare continents. This difference prevails when vegetation is allowed to adjust to and interact with climate. Further simulations with initial surface conditions that differ in the region of the Asian desert only indicate that local feedback processes are less important in the development of multiple states. In the interglacial, pre-industrial climate, multiple states develop only in the Sahel region. There, local climate-vegetation interaction seems to dominate.

Clariy aim

Updated major findings

1 Introduction

The interaction between atmosphere and vegetation may allow for multiple equilibria of the system pointing to intransitive dynamics in the climate system is as suggested by Lorenz (1968). Multiple equilibrium states have been detected in various model simulations when initialised with different

vegetation covers. Claussen (1994), Claussen and Gayler (1997), Claussen (1998), Kubatzki and Claussen (1998), Wang and Eltahir (2000), Zeng and Neelin (2000), and Rachmayani et al. (2015) find multiple states in Northern Africa, Oyama and Nobre (2003) in the Amazon region, Claussen (1998) in Central Asia, and Dekker et al. (2010) in the northern high latitudes. In all cases, simulations with initially more extended vegetation cover lead to a moister climate and smaller deserts than simulations initialised with sparse vegetation coverage.

Studies which focus on palaeoclimates indicate that the stability of the climate-vegetation system depends on the climate state. For example, the intransitivity of the climate-vegetation system over Northern Africa vanishes, or becomes much less pronounced, for the mid-Holocene climate in the simulations by Claussen and Gayler (1997) and Rachmayani et al. (2015), respectively. Likewise, Bathiany et al. (2012) show that the pattern of bi-stability over Northern Africa changes at different times in different locations during the transition from mid to late Holocene. Such changes in the stability of the climate-vegetation system may lead to abrupt changes in vegetation and climate due to a loss of stability in the regions which exhibit multiple states (Brovkin et al. 1998; Claussen et al. 1999; Renssen et al. 2003). Further, changes in the stability of the climate-vegetation system may even induce abrupt changes in locations which seem to be more stable, but which are interlinked with the unstable locations (Bathiany et al. 2013a, Bathiany et al. 2013b).

So far, most studies have assessed the stability of the climate-vegetation system for interglacial or glacial climate, i.e. for climate states with permanent ice sheets. Little is known about the transitivity of the climate-vegetation system in climates that strongly differ from the current late Quaternary climate. Therefore, we explore the stability of the climate-vegetation system in a much warmer climate than the present one which does not support permanent ice sheets and sea ice.

During the early Eocene (about 54 to 52 Ma ago) such a warm, almost ice-free climate prevailed. An atmospheric CO_2 concentration between 300 ppm and 2000 ppm (Beerling and Royer 2011) as well as the specific distribution of continents and bathymetry led to 5°C to 6°C warmer tropics (Pearson et al. 2007) and to mostly ice-free poles (Zachos et al. 1992). The warm climate allowed a dense vegetation cover in almost all regions (Willis and McElwain 2002). Even on Antarctica and in the high North, flora fossils indicate a dense tree cover (Wolfe 1985; Eberle and Greenwood 2012; Harrington et al. 2012; Pross et al. 2012).

We perform simulations with the Earth system model of the Max Planck Institute for Meteorology (MPI-ESM) and assume continents, bathymetry, and atmospheric CO_2 concentration according to the early Eocene. Other boundary conditions such as orbital parameters, atmospheric methane, and nitrous oxide as well as the assumed plant species in the dynamic vegetation module are the same as in pre-industrial simulations. The resulting simulated climate matches temperature reconstructions of the early Eocene fairly well. Only in the high latitudes, the simulated near-surface temperature is lower than reconstructions suggest. Despite this mismatch, the simulated Eocene-like climate fulfills

Clarify our aim

our demand because we rather aim to investigate the stability of the climate-vegetation system in a warm almost ice-free climate than to reproduce the climate of the early Eocene as well as possible.

To compare the stability of the climate-vegetation system in the warm Eocene-like climate and in the pre-industrial climate, we perform the same experiment with boundary conditions for both these climates. The respective experiments contain two simulations each which start from different vegetation states: All ice-free continents are either completely covered with dense forests or with bare-soil deserts, respectively. From these initial states, the model system is allowed to freely evolve, with dynamically interacting atmosphere, ocean, and vegetation. Depending on the initial conditions, new equilibria in the climate-vegetation system are reached after some 1000 years of simulation.

2 Experiment

2.1 Model

The Earth system model of the Max Planck Institute for Meteorology (MPI-ESM) consists of the atmospheric general circulation model ECHAM6 (Stevens et al. 2013), the Max Planck Institute Ocean Model MPIOM (Jungclaus et al. 2013), the land surface scheme JSBACH (Reick et al. 2013), and the ocean biogeochemistry model HAMOCC (Ilyina et al. 2013). We use ECHAM6 in a horizontal resolution is T31 (approximately 3.75°) and with 31 levels in the vertical. The ocean grid has a horizontal resolution of about 3° and 40 levels in depth. JSBACH includes a dynamic vegetation module based on a tiling approach (Brovkin et al. 2009). Vegetation is represented by eight Plant Functional Types (PFTs) which reflect present-day plant taxa (Tab. 1).

We perform the same simulations for an interglacial climate and a warm ice-free climate. To get an interglacial climate, we assume pre-industrial boundary conditions for the chemical composition of the atmosphere, orbital parameters, continents, orography, and bathymetry (Tab. 3). To achieve a warm ice-free climate, we use the boundary conditions which Heinemann et al. (2009) use for their Eocene simulation. Like they do, we prescribe the orography and bathymetry maps by Bice and Marotzke (2001). The orography map lacks information on sub-grid orography such as slope, anisotropy, orientation, standard deviation, maximum, minimum, and mean elevation. Without these information, sub-grid interactions of atmospheric flow with orography can not be parameterised in ECHAM6 (Stevens et al. 2013). Hence, we turn off the module for sub-grid orographic drag and wave generation.

Reformulate experiment explanation to avoid the implication that the study focuses on the early Eocene climate

In the standard version of MPIOM, the grid poles are over Greenland and Antarctica. With Eocene continents, the pole over present-day Greenland coincide with the Palaeo-Atlantic Ocean, i.e. meridians converge at this pole leading to numerical singularities. To avoid singularities, we use the setting by Heinemann et al. (2009) who placed the MPIOM north pole and south pole to the large continents of Palaeo-Asia and to Palaeo-South America, respectively.

The atmospheric CO_2 concentration is fixed to 560 ppm (Tab. 2), which is the lower limit of reconstructions (Zachos et al. 2001 and Beerling and Royer 2011). With a fixed atmospheric CO_2 concentration, carbon pools does not need to reach an equilibrium which would take several thousand year. Instead, living biomass responses to a constant atmospheric CO_2 and equilibrates already after several decades. Since our simulations run for 1000 years, this time span is long enough to reach an equilibrium in living biomass.

Clarify handling of carbon pools

The other greenhouse gases methane and nitrous oxide are set to pre-industrial values in the early Eocene atmosphere and also the orbit corresponds to the pre-industrial orbit (Tab. 2). Soil properties are the same as in the pre-industrial simulations and represent clay. Soil dynamics are not considered, i.e. soils remain constant over the whole simulations.

Explain soil properties

During the early Eocene, plant species have been differed from today. For instance, grass land is common today, but evolved after the early Eocene (Willis and McElwain 2002). C_3 spread in the early to mid Miocene (20 - 10 Ma) (Janis 1993), while C_4 expanded during the mid to late Miocene (Cerling et al. 1993). Instead, other plant species dominated the vegetation cover during the early Eocene which are extinct, or almost extinct, today such as paratropical rainforest or polar forest (Wolfe 1985). We neglect any differences in plant taxa to isolate the geographic and climatic factors affecting the stability of the climate-vegetation system.

Emphasise the focus on geographic and climatic factors and the exclusion of physiological factors

To initialise our Eocene simulations, we perform a simulation starting from the equilibrium Eocene climate by Heinemann et al. (2009). Like in their simulation, we assume a savannah vegetation with a desert cover of 40 %, a tree cover of 24 %, and a grass cover of 36%. After 300 years, near-surface temperature and upper-level ocean temperatures are in equilibrium. Only in the deep ocean, a marginal temperature trend remains.

2.2 Simulations

Starting from the equilibrium Eocene climate, we perform two simulations. In the first 400 years of the simulations, vegetation is fixed to dense forest in the FE_f simulation and to bare soil in the DE_f simulation. After that period, the forest world and desert world simulation continue with a dynamically evolving vegetation cover in the FE_d simulation and in the DE_d simulation, respectively.

In order to separate the albedo effect of vegetation from the hydrological effect, we perform the initial desert simulation and the initial forest simulation two times, respectively. All soils either have a homogeneous albedo of 0.1 (dark soil) or 0.4 (bright soil). In the dark soil case, soil and vegetation have about the same albedo leading to weak albedo changes by vegetation relative to bare soil. In other words, vegetation affects climate mainly through the hydrological cycle. In the bright soil case, vegetation has a much lower albedo than soil. Hence, both, the albedo effect and the hydrological effect of vegetation act. In the bright-soil simulations, the climate-vegetation system reaches the same state when initialised with dense forest as when initialised with bare soil. As we focus on intransitive dynamics in the climate-vegetation system, we exclude a detailed discussion of

the bright-soil simulations in this study. Instead, we present the results for the dark-soil simulations where multiple equilibria establish depending on the initial vegetation cover in the warm ice-free climate. Table 3 gives an overview of the considered four simulations where all soils have a low soil albedo.

Introduce the additional simulations

To analyse the local impact of initial vegetation cover on the intransitivity, we perform two additional simulations with Eocene boundary conditions. In the DA_f simulation, we fix the vegetation cover to bare soil in Central Asia and to forests elsewhere and simulate 400 years. Starting from the DA_f simulation, we let the vegetation evolve dynamically in the DA_d simulation. Analogously, we assume a dense forest in Central Asia and deserts elsewhere in the FA_f simulation. After 400 years with a fixed vegetation cover, vegetation evolves dynamically in the FA_d simulation.

Analogue to the Eocene simulations, we perform two pre-industrial simulations. The FP_f simulation runs for 400 years with a fixed forest cover on all ice-free continents. Afterwards, vegetation establishes dynamically in the FP_d simulation. In the DP_f simulation, vegetation is fixed to desert for 400 years. Starting from the DP_f simulation, vegetation evolves dynamically in the DP_d simulation.

3 Warm almost ice-free climate and its vegetation cover

Compare simulated Eocene temperature with reconstructions

Near-surface temperature in the DE_d simulation agrees with temperature reonstructions of the early Eocene temperature in the topics and subtropics. In the northern mid to high latitudes, the DE_d simulation is colder than reconstructions of Eocene temperatures (Fig. 1). Relative to the TEX_{86} estimate by Sluijs et al. (2006) north of Greenland, the simulated sea-surface temperature (SST) is even 18 K lower. The TEX_{86} estimate, however, likely represents summer temperatures (Sluijs et al. 2006). Considering summer values, the DE_d simulation is 15 K colder than temperature estimates suggest for the early Eocene.

In the southern high latitudes, the simulation agrees with marine and terrestrial temperature estimates. The only exception is the SST reconstruction by Bijl (2009) that suggests temperature of 24°C at the Tasman Plateau (Fig. 1). Like the estimate by Sluijs et al. (2006), the estimate by Bijl (2009) is based on TEX_{86} and likely has a bias to summer temperatures. Considering the summer temperature, our simulation is colder than the reconstruction by 9 K over the southern Pacific Ocean.

Introduce the simulated warm climate

Despite the mismatch of our simulated early Eocene climate with reconstructions in the high latitudes, the simulation fullfills our demands for a warm ice-free climate. At the end of the DE_d simulation, global mean temperature is 7.1 K higher than at the end of the pre-industrial DP_d simulation. The temperature difference is most pronounced in the high latitudes where the DE_d climate is warmer than the DP_d climate by 34.5 K south of 70°S and 10.3 K north of 70°. In the tropics, the temperature difference is 5.4 K leading to a weaker pole-to-equator temperature gradient in the DE_d climate than in the DP_d climate. With above freezing temperatures during most time of the year even in the high latitudes, permanent ice is absent and sea ice occurs only seasonally in the Arctic Ocean.

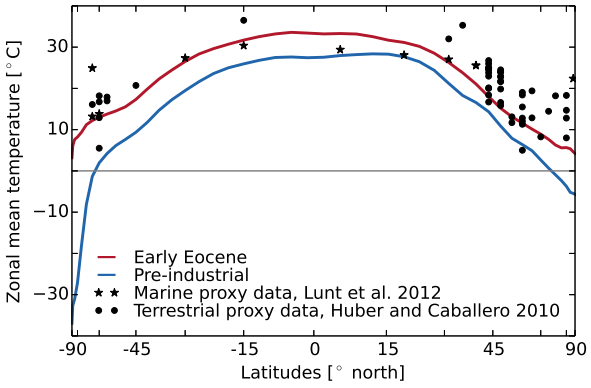

Figure 1. Zonal annual mean 2-m temperature in the DE_d simulation (red line) and in the DP_d simulation (blue line). Stars show estimates of annual-mean sea-surface temperature (SST) and near-surface temperature for the early Eocene based on $\delta^{18}O$, Mg/Ca, and TEX_{86} (Lunt et al. 2012). Cycles refer to terrestrial annual mean temperature estimates based on macrofloral and palynoflora assemblage data and from teeth, hydrogen isotopes, and oxygen isotopes (Huber and Caballero 2011).

The hydrological cycle is enhanced in the DE_d climate with 15 % stronger precipitation than in the DP_d climate.

Evaluate vegetation cover

In the warm and humid Eocene-like climate, MPI-ESM simulates a dense vegetation cover which matches vegetation reconstructions in the high latitudes (Fig. 2). Like the flora fossil assemblage by Utescher and Mosbrugger (2007) suggests, extra-tropical trees cover Antarctica and reach the Arctic Ocean in the High North at the end of the DE_d simulation. Beside trees, our model simulates plenty C_3 grass in the mid to high latitudes. The grass cover disagrees with reconstruction because wide-spread grassland likely evolved after the early Eocene, between the late Eocene (Bouchenak-Khelladi et al. 2010) and the early to mid Miocene (20-10 Ma) (Janis 1993). C_3 grass is a common PFT in JSBACH and we decided to stay with it despite the discrepancy to the Eocene plant taxa. This approach excludes the influence of characteristic Eocene plant taxa on the stability of the climate-vegetation system and reveals the sensitivity of the stability to geophysical boundary conditions (continents, bathymetry, and atmospheric CO_2).

Tropical forest is bounded between 30°S and 30°N in the DE_d simulation but reconstructions suggest a poleward extent up to 60°S and 60°N during the early Eocene (Fig. 2) (Wolfe 1985, Willis and McElwain 2002, Utescher and Mosbrugger 2007) . We assume that the mismatch results from the cold bias in the simulated high latitude temperature discussed above. C_4 grass coexist with tropical forest in the tropics in the DE_d simulation, but the C_4 pathway evolved and expanded during the late Miocene (Cerling et al. 1993). Like for C_3 grass, we decided to stay with C_4 grass to limit the difference between the Eocene simulations and the pre-industrial simulations to differences in continents, bathymetry, and atmospheric CO_2.

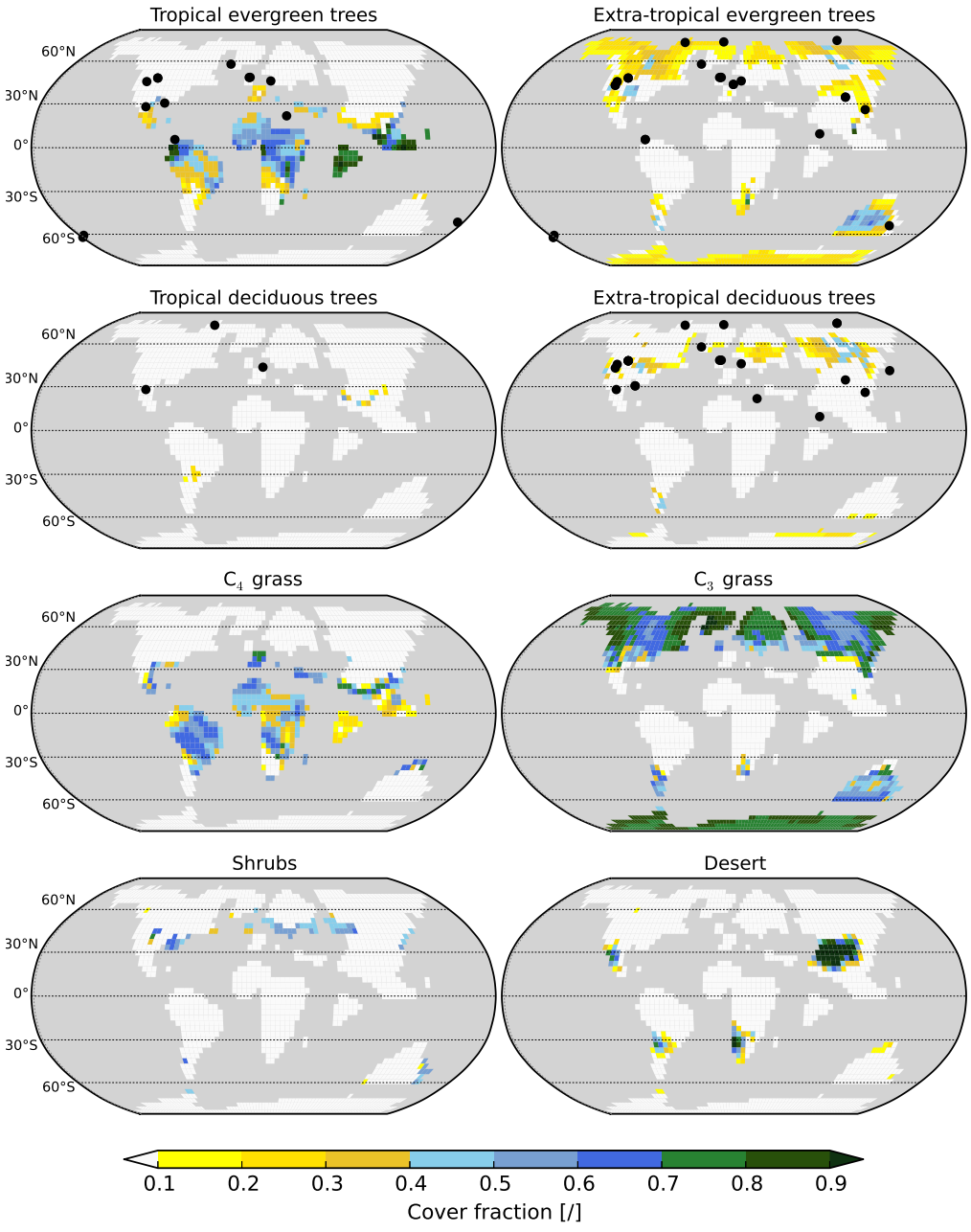

Figure 2. Simulated vegetation cover in the DE_d simulation and reconstructed vegetation based on the flora collection by Utescher and Mosbrugger (2007). Locations are marked where the diversity of the respective PFT in flora collection exceeds 10%.

185 In general, deserts are suggested to have been rare in the warm climate of the early Eocene (Willis and McElwain 2002). Only in Central Asia, sediments and flora fossils indicate semi-dry to dry conditions with desert vegetation (Wang et al. 2013 and Quan et al. 2012). Like previous simulations by Huber and Caballero (2011) and Loptson et al. (2014), our simulation reproduces the Asian desert

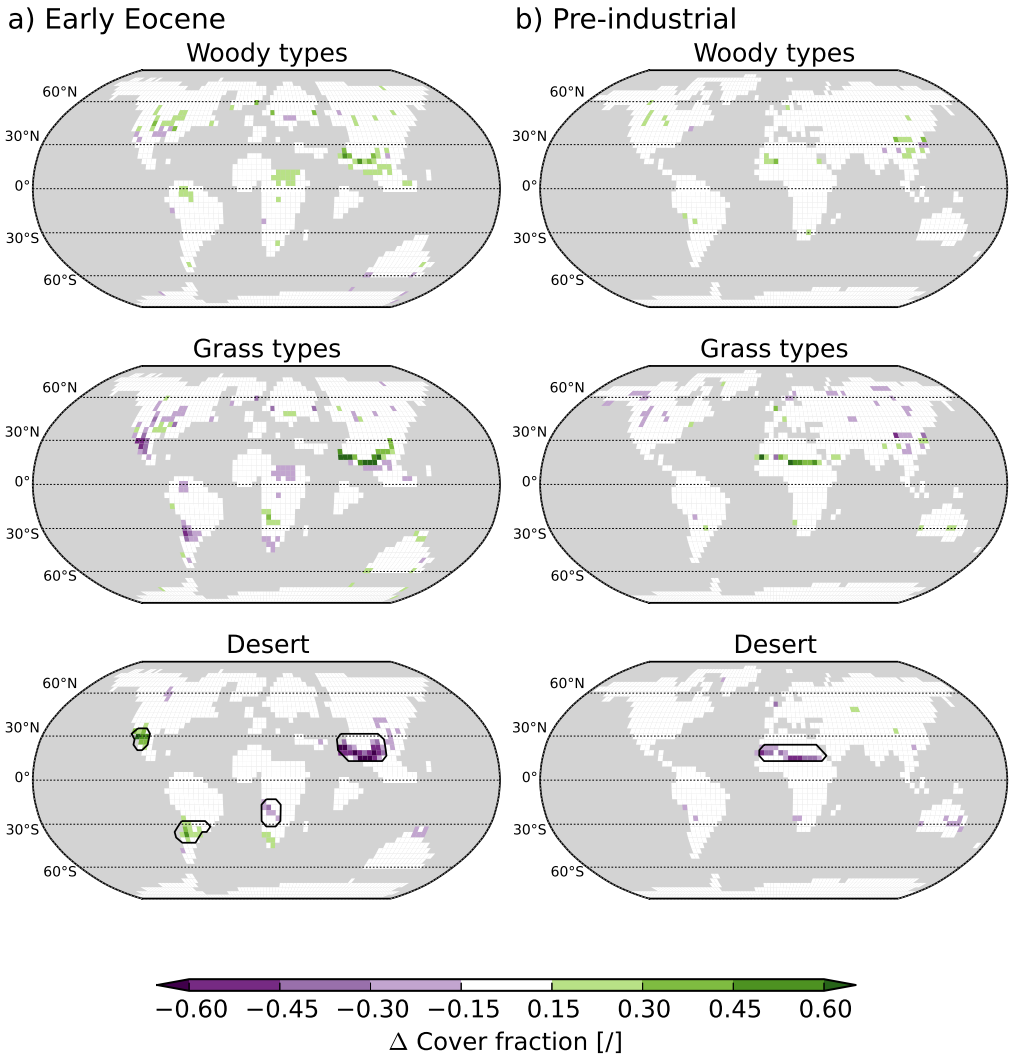

Figure 3. Differences in vegetation cover between the simulations that start from a forest world and the simulations that start from a desert world. Shown are differences for the early Eocene climate (FE_d - DE_d) (a) and for the pre-industrial climate (FP_d - DP_d) (b). Mapped differences refer to the average over 30 years and are significant on a 95% level. Woody types include all trees and shrubs. Grass types refer to C_4 grass and to C_3 grass. Black contour lines mark regions which are analysed in more detail in Fig. 4 and Fig. 9.

because a monsoon climate causes a seasonally dry climate in this region. In subtropical Africa and America, further small deserts and semi-desert evolve in the DE_d simulation.

Stronger title to emphasise the focus on multi-stabilities

4 Results and Discussion

4.1 Bi-Stable deserts in the Eocene climate

The warm and humid early Eocene climate favours a dense vegetation cover in almost all regions. Only in Central Asia and in southern Africa, deserts remain in the DE_d simulation (Fig. 2), and subtropical semi-deserts establish in South America, North America, and Australia. In these arid and semi-arid regions, pronounced differences in vegetation cover emerge between the DE_d simulation and the FE_d simulation (Fig. 3).

Remove the hypothesis of a local hydrological feedback

The difference in the vegetation cover is most pronounced in the Asian desert (region marked in Fig. 3). At the southern edge of the desert, more grass and trees remain in the FE_d simulation than in the DE_d simulation because precipitation is stronger. At the end of the FE_d simulation, precipitation in Central Asia is 1.58 mm/day stronger and desert cover is 0.36 smaller (Fig. 4 a). Also in the semi-desert in southern Africa, desert cover is smaller at the end of the FE_d simulation than at the end of the DE_d simulation (Fig. 4 d).

In the semi-desert in western North America, precipitation is smaller by 0.52 mm/day (70%) at the end of the FE_d simulation than at the end of the DE_d simulation. In the drier climate, desert cover is larger by 0.43 (Fig. 4 c). Also in the semi-desert in southern South America, a weaker precipitation in the FE_d simulation results in a larger desert cover than in the DE_d simulation (Fig. 4 b). The differences on the American continents are counterintuitive because starting from dense forest leads to a larger desert in these regions than starting from bare soil. This result disagrees with all simulations previously mentioned in the introduction. Later, we will discuss the mechanism causing these bi-stabilities.

To identify the driving mechanisms for the multiple steady vegetation states, we analyse the large-scale atmospheric circulation. Following Claussen (1997), we compute the velocity potential at 200 hPa which is an indicator of large-scale upper-air divergence and convergence, and hence, convection and subsidence in the tropics. The separation of the horizontal wind, $\boldsymbol{V}$, in the rotational component, $\boldsymbol{V}_\Psi$, and in the divergent component, $\boldsymbol{V}_\chi$, yields

$$\boldsymbol{V} = \boldsymbol{V}_\Psi + \boldsymbol{V}_\chi. \tag{1}$$

The divergent part of the horizontal wind is the gradient of the velocity potential, χ,

$$\boldsymbol{\nabla}\chi = \boldsymbol{V}_\chi. \tag{2}$$

Hence, the divergent part of the large-scale horizontal wind is directed towards the strongest increase in the velocity potential. This relation implies that air flows from the centre of negative velocity potential to the centre of positive velocity potential. Therefore, upper air diverges in the centre of negative velocity potential and converges in the centre of positive velocity potential. Below the divergence, air rises and below the convergence, air subsides.

Figure 5 shows the velocity potential in the desert world, DE_f, and in the forest world, FE_f, at 200 hPa averaged over the last 30 years of the simulations. In the desert world, the centre of posi-

tive velocity potential indicates strong subsidence over the tropical Atlantic Ocean, and the centre of negative velocity potential implies convection over the tropical Pacific Ocean (Fig. 5 a). In the forest world, the centre of subsidence intensifies and shifts to northern South America relative to the circulation in the desert world, and the centre of convection intensifies and shifts to the western Pacific Ocean (Fig. 5 b).

Remove hypothesis of a global teleconnection triggered by the Asian desert

Starting from the desert world simulation and the forest world simulation, vegetation cover evolves dynamically with climate during the DE_d simulation and the FE_d simulation, respectively. The initial large-scale atmospheric circulation pattern, however, persists (Fig. 5 c, d). Hence, at the end of the simulations, the atmospheric circulation still differs strongly between the DE_d simulation and the FE_d simulation. With stronger convection over the west Pacific Ocean in the FE_d simulation, precipitation at the southern edge of the Asian desert is stronger than in the DE_d simulation leading a smaller desert cover. Over the American continents where subsidence strengthens relative to the DE_d simulation, the subtropical semi-arid regions are drier, and desert cover is larger.

Present new results

In the desert world, a temperature gradient occurs above 100 hPa between cold air above the tropics and warmer air above the mid and high latitudes (Fig. 7). This meridional temperature gradient induces a weak easterly wind at about 5°N due to the thermal wind relation (Fig. 7). In the forest world, near-surface temperature is reduced relative to the desert world, and in the colder climate,

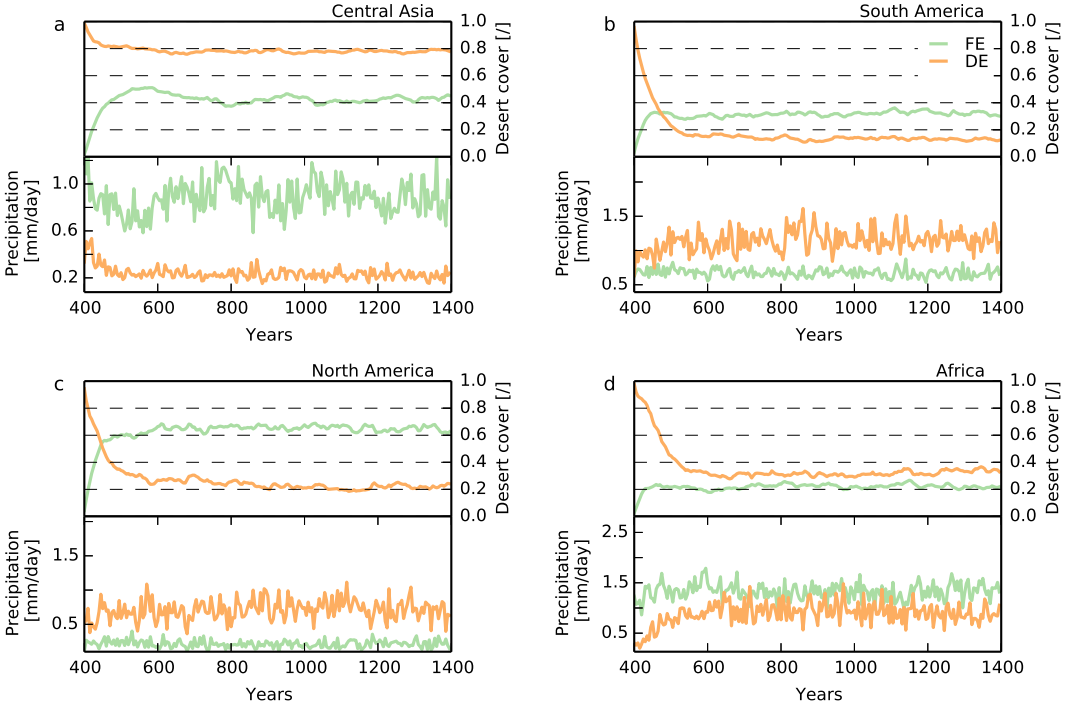

Figure 4. Time series of five-year mean desert cover and precipitation in selected regions in Central Asia (a), South America (b), North America (c), and Africa (d) in the FE_d simulation (green line) and in the DE_d simulation (orange line). The regions are marked in Fig. 3.

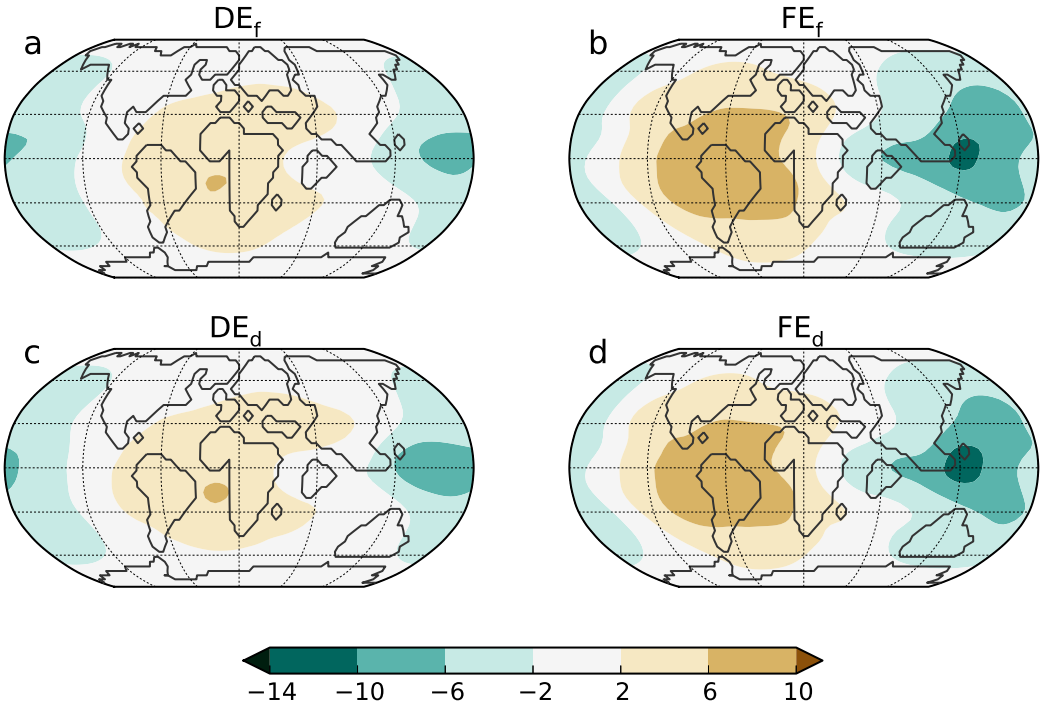

Figure 5. Velocity potential at 200 hPa at the end of the desert world simulation (a), forest world simulation (b), DE_d simulation (c), and FE_d simulation (d). The average over the last 30 years of the respective simulation is considered. The DE_d simulation and the FE_d simulation start from the desert world simulation and the forest world simulation, respectively. Brown colours indicate to a positive velocity potential, upper-air convergence, and subsidence. Green colours indicate to a negative velocity potential, upper-air divergence, and rising.

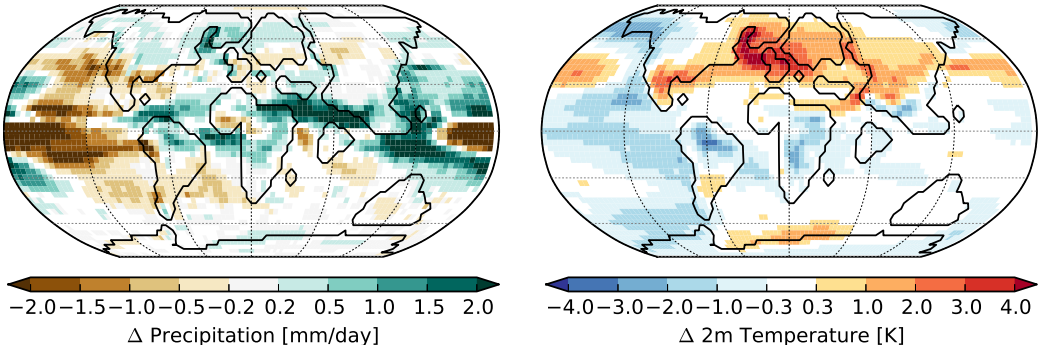

Figure 6. Differences in precipitation and 2-m temperature between the FE_d simulation and the DE_d simulation. The average over the last 30 years of the simulations is considered. Depicted differences are significant on a 95% level.

tropopause is lower leading to a warming at the tropopause. The tropopause decline and the connected the warming reach 200 hPa in the mid and high latitudes and 100 hPa in the tropics. Due to

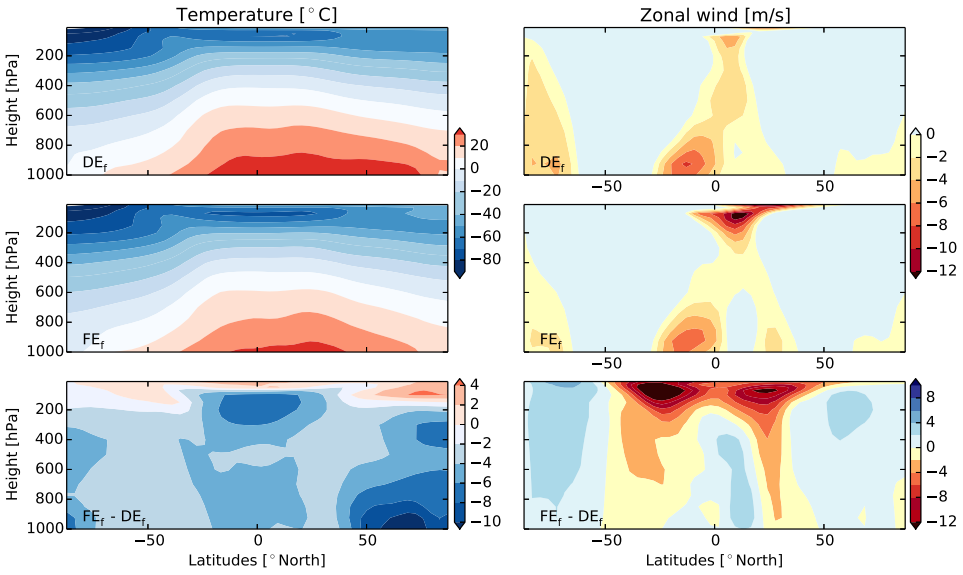

Figure 7. Zonal-mean temperature and wind in the desert world simulation, DE_f, and in the forest world, FE_f, simulation of the early Eocene climate. Further, the differences between the forest world simulation and the desert world simulation (FE_f - DE_f) is shown. The average over July and August in the last 30 years of the simulations is considered.

the weaker warming in the tropics than in the mid to high latitudes, the meridional temperature gradient between tropics and mid to high latitudes enhances relative to the desert world. With a stronger meridional temperature gradient, the easterly wind at 100 hPa strengthens in the forest world.

The stronger easterly wind in the forest world transports more air from the convection zone over Asia to the subsidence zone over America than in the desert world. The enhanced air transport manifests in an intensified velocity potential pattern and a general westward shift relative to the desert world (Fig. 5). This result suggests that forest affects large-scale atmospheric circulation by reducing near-surface temperature, lowering tropopause height, and thereby, enhancing the easterly wind at the tropopause.

During the FE_d simulation, the warming in the height becomes weaker but the easterly wind is still stronger than in the DE_d simulation and supports the intensified and shifted velocity potential pattern (not shown here). The persistence of the stronger easterly wind in the FE_d simulation again indicates that the initial forest cover shifts the atmospheric circulation to another self-preserving state than the desert cover.

To test whether large-scale or local initial vegetation causes the bi-stability in the climate-vegetation system, we perform two additional simulations. In the Asian Desert simulation, DA_f, we fix the vegetation cover to a desert in Central Asia (marked region in Fig. 8) and to forests elsewhere and simulate 400 years. After that, we let the vegetation evolve dynamically during the DA_d simulation.

Present results from the additional simulations

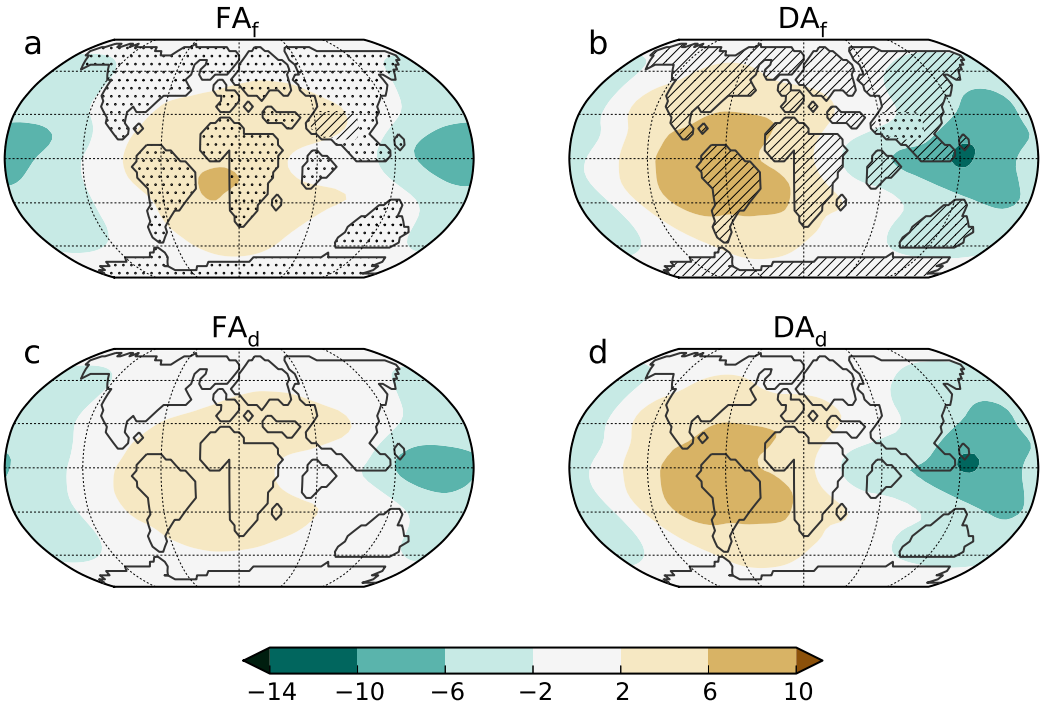

Figure 8. Velocity potential at 200 hPa at the end of the FA_f simulation and DA_f simulation (a-b), and at the end of the FA_d simulation and DA_d simulation (c-d). The average over the last 30 years of the respective simulation is considered. Brown colours indicate to a positive velocity potential, upper-air convergence, and subsidence. Green colours indicate to a negative velocity potential, upper-air divergence, and rising.

Analogously, we assume a dense forest in Central Asia and deserts elsewhere in the Asian Forest simulation, FA_f. After 400 years with a fixed vegetation cover, vegetation evolves dynamically in the FA_d simulation.

In the DA_f simulation, when vegetation is fixed, the atmospheric circulation reaches the same state as in the forest world. Then, vegetation evolves dynamically and the circulation pattern persists ending up in the same stable state as in the FE_d simulation. Analogously, the FA_f simulation yields the same large-scale atmospheric circulation as the desert world simulation. With a dynamically evolving vegetation cover, the atmospheric circulation persists leading to the same state in the FA_d simulation as in the DE_d simulation. The agreement of the DA_d simulation with the FE_d simulation and the FA_d simulation with the DE_d simulation shows that local initial vegetation fails to cause multiple climate-vegetation states. Instead, our results suggest that large-scale initial vegetation cover causes multipe climate-vegetation states in the warm, ice-free climate.

4.2 Bi-stable Sahel in the pre-industrial climate

In the pre-industrial climate, the vegetation difference between the FP_d simulation and the DP_d simulation is restricted to the Sahel. More vegetation remains in this region and the desert cover is smaller by 0.21 in the FP_d simulation than in the DP_d simulation. Consistently, precipitation is about two times larger in the FP_d simulation than in the DP_d simulation (Fig. 11).

In contrast to the Eocene simulations, the large-scale atmospheric circulation, as indicated by the 200 hPa velocity potential, differs only slightly between the forest world simulation and the desert world simulation for pre-industrial climate (Fig. 10 a, b). When vegetation is allowed to dynamically adjust to and to interact with climate, the small differences in the large-scale atmospheric circulation between the initially forested world and the initially deserted world nearly vanish (Fig. 10 c, d). The weak impact of initial vegetation on the large-scale atmospheric circulation implies that a local effect rather than a large-scale effect leads to multiple climate-vegetation states in the pre-industrial Sahel climate.

Present results of extended analysis

In the Sahel, evapotranspiration amounts to 1.1 mm/day in the FP_d simulation and 0.64 mm/day in the DP_d simulation. Cloud cover is larger, less solar radiation reaches the surface and latent heat flux is larger by a factor of 1.7 in the FP_d simulation than in the DP_d simulation. Consistently, a stronger meridional temperature gradient develops with warmer air over the Sahara and colder air over the Sahel in the FP_d simulation than in the DP_d simulation (Fig. 11). The increased temperature gradient enhances the African Easterly Jet (AEJ) at 700 hPa in the FP_d simulation (Fig. 12). Stronger AEJ over moister or greener Sahel region is in line with earlier simulations by Cook (1999) and Rachmayani et al. (2015), respectively. The stronger AEJ is accompanied with a stronger horizontal moisture flux convergence (Fig. 12) which, in turns leads to larger precipitation over the Sahel in the FP_d simulation than in the DPd simulation (Fig. 11).

In the studies by Claussen and Gayler (1997) and Claussen (1998), strong differences in surface albedo triggered multiple stable vegetation–atmosphere states in the Sahara and Sahel. In our study,

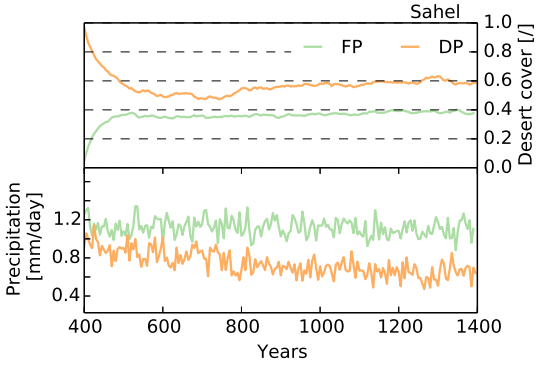

Figure 9. Time series of five-year mean desert cover and precipitation in pre-industrial Sahel in the FP_d simulation (green line) and in the DP_d simulation (orange line). The Sahel region is marked in Fig. 3.

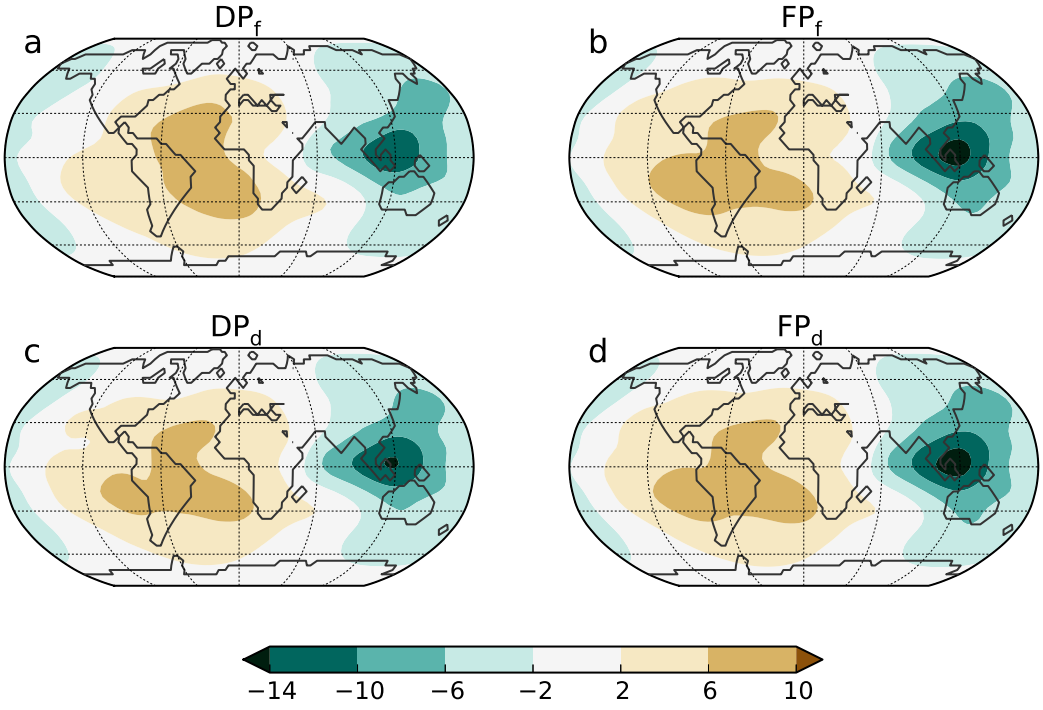

Figure 10. Velocity potential at 200 hPa at the end of the desert world simulation (a), the forest world simulation (b), the DP_d simulation (c), and the FP_d simulation (d). The average over the last 30 years of the respective simulation is considered. The DP_d simulation and the FP_d simulation start from the desert world simulation and the forest world simulation, respectively. Brown colours indicate to a positive velocity potential, upper-air convergence, and subsidence. Green colours indicate to a negative velocity potential, upper-air divergence, and rising.

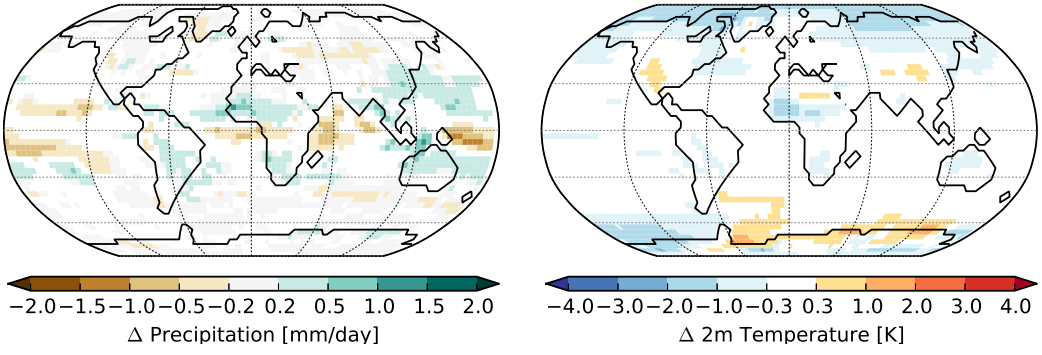

Figure 11. Differences in precipitation and 2-m temperature between the end of the FD_P simulation and the end of the DD_P simulation. Depicted differences are significant on a 95% level.

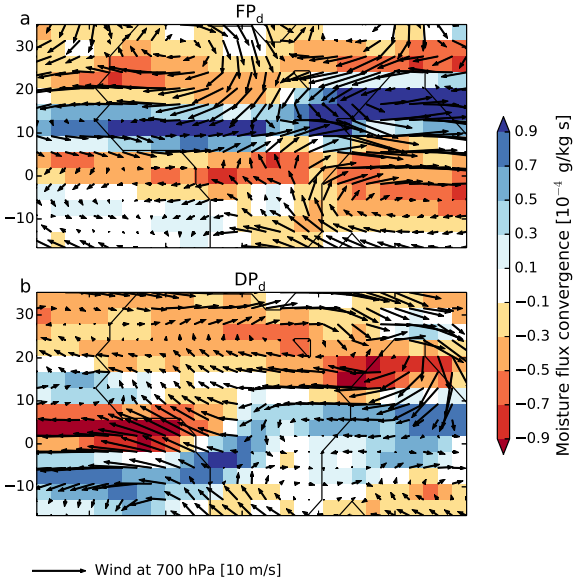

Figure 12. Horizontal wind at 700 hPa averaged over July, August, September in the last 30 years of the FP_d simulation and DE_d simulation. Shaded colors show the moisture flux convergence.

albedo differences are assumed to be small. Hence.a hydrological feedback causes multiple states as it is the case in the simulations by Rachmayani et al. (2015).

Reformulate conclusions to include new findings

5 Conclusion

To our knowledge, the transitivity of the global climate-vegetation system has so far been explored for late Quaternary climate, i.e., glacial, interglacial mid-Holocene and present-day climate. Therefore, we extend the analysis to early Eocene conditions, i.e., to a warm, almost ice-free climate with a different configuration of continents than today. To this end, we initialise the simulations by prescribing either dense forests or bare deserts on all continents both for early Eocene and pre-industrial climate. For early Eocene conditions, multiple equilibrium states evolve: starting with desert continents, an extended desert remains in Central Asia. Starting with complete forest cover, the Asian desert is much smaller, while coastal deserts develop in the Americas which appear to be larger than in the simulations with initially bare continents. We attribute these differences to differences in the large-scale atmospheric circulation. With initially forested continents, a stronger dipole in the 200 hPa velocity potential develops than in the simulation with initially bare continents. This difference prevails when vegetation is allowed to interact with climate.

Additional simulations with initial surface conditions that differ in the region of the Asian desert only indicate that local feedback processes are less important for the development of multiple states. When initialising a simulation with a patch of Asian desert in an otherwise completely forested

world leads to mainly the same equilibrium as when the simulation is initialised with completely forested continents. The same is valid, if a patch of Asian forest is prescribed in simulations with initially bare continents. It would be interesting to find the spatial extent of the initial perturbation, or the repellor, over the Asian continent from which the system is driven into different modes.

In the pre-industrial climate, local vegetation-precipitation feedbacks seem to cause multiple equilibrium climate-vegetation states which are restricted to the Sahel region. In the simulations with large-scale initial forest cover, forests cool the Sahel in comparison with the simulations with initially bare continents. This cooling is associated with stronger latent heat flux and stronger cloud cover. The difference in local cooling results in a stronger meridional temperature gradient between cold air above the Sahel and warmer air above the Sahara. The difference in the meridional temperature contrast, in turn, fuels the African Easterly Jet which transports moisture to the Sahel and thereby supports vegetation growth in the simulation with initial forested continents. Hence, in these simulations, and in line with previous studies (e.g., Rachmayani et al., 2015), it is a local hydrological climate-vegetation feedback which leads to multiple equilibria over the Sahel region in the pre-industrial climate.

In our study, we focused on biogeophysical processes and associated intransitivity of the climate-vegetation system. We neglected any differences between plant taxa and used pre-industrial plant functional types (PFTs) for the early Eocene climate simulation. The strongest discrepancy between Eocene plant taxa and the used PFTs concerns grasses. JSBACH considers C_3 grass and C_4, but C_3 grasses occurred rarely during the early Eocene and C_4 grasses did not exist at all. To solve this discrepancy, one might exclude C_4 grasses and replace C_3 grasses by fern and herbs which grew plentifully during that time (Utescher and Mosbrugger (2007)). Assuming fern and herbs instead of C_3 grass, we expect that fern and herbs would spread in the region where we have simulated C_3 grass before because JSBACH only distinguishes between woody vegetation, i.e. trees and shrubs, and non-woody vegetation, i.e. every species except trees and shrubs. Presumably, JSBACH would handle fern and herbs in the same way as it handles grass. By allowing fern and herbs to grow in tropical temperatures, we assume that fern and shrubs would also capture the niche of C_4 grass.

Acknowledgments

We thank Veronika Gayler and Helmuth Haak (Max Planck Institute for Meteorology) for technical support, and Torsten Utescher and Matthew Huber for providing the data to compare our modelling results with. The constructive critique of the anonymous reviewers, specifically the decisive question on local feedbacks in the early Eocene simulations, helped to improve our paper. This work used computational resources by Deutsches Klima Rechenzentrum (DKRZ) and was supported by the Max Planck Society (MPG).

References

Bathiany, S., Claussen, M., , and Fraedrich, K. (2012). Implications of climate variability for the detection of multiple equilibria and for rapid transitions in the atmosphere-vegetation system. *Climate Dynamics*, 38:1775–1790.

Bathiany, S., Claussen, M., and Fraedrich, K. F. (2013a). Detecting hotspots of atmosphere-vegetation interaction via slowing down. part 1: A stochastic approach. *Earth System Dynamics*, 4:63–78.

Bathiany, S., Claussen, M., and K. Fraedrich, K. (2013b). Detecting hotspots of atmosphere-vegetation interaction via slowing down - part 2: Application to a global climate model. *Earth System Dynamics*, 4:79–93.

Beerling, D. and Royer, D. (2011). Convergent Cenozoic CO_2 history. *Nature Geoscience*, 4(7):418–420.

Bice, K. L. and Marotzke, J. (2001). Numerical evidence against reversed thermohaline circulation in the warm Paleocene/Eocene ocean. *Journal of geophysical research*, 106(C6):11529–11542.

Bijl, P. K. (2009). Early palaeogene temperature evolution of the southwest pacific ocean. *Nature*, 461:776–779.

Bouchenak-Khelladi, Y., Verboom, G. A., Savolainen, V., and Hodkinson, T. R. (2010). Biogeography of the grasses (poaceae): a phylogenetic approach to reveal evolutionary history in geographical space and geological time. *Botanical Journal of the Linnean Society*, 162:543–557.

Brovkin, V., Claussen, M., Petoukhov, V., and Ganopolski, A. (1998). On the stability of the atmosphere-vegetation system in the sahara/sahel region. *Journal of Geophysical Research: Atmospheres*, 103(D24):31613–31624.

Brovkin, V., Raddatz, T., and Reick, C. H. (2009). Global biogeophysical interactions between forest and climate. *Geophysical Research Letters*, 36:L07405.

Cerling, T., Wang, Y., and Quade, J. (1993). Expansion of C4 ecosystems as an indicator of global ecological change in the late Miocene. *Nature*, 361(6410):344–345.

Claussen, M. (1994). On coupling global biome models with climate models. *Climate Research*, 4:203–221.

Claussen, M. (1997). Modeling bio-geophysical feedback in the african and indian monsoon region. *Climate dynamics*, 13(4):247–257.

Claussen, M. (1998). On multiple solutions of the atmosphere-vegetation system in present-day climate. *Global change biology*, 4(5):549–559.

Claussen, M. and Gayler, V. (1997). The greening of the sahara during the mid-holocene: Results of an interactive atmosphere-biome model. *Global Ecology and Biogeography Letters*, 6(5):pp. 369–377.

Claussen, M., Kubatzki, C., Brovkin, V., Ganopolski, A., Hoelzmann, P., and Pachur, H.-J. (1999). Simulation of an abrupt change in saharan vegetation in the mid-holocene. *Geophysical Research Letters*, 26(14):2037–2040.

Cook, K. H. (1999). Generation of the african easterly jet and its role in determining west african precipitation. *Journal of Climate*, 12:1165–1184.

Dekker, S. C., de Boer, H. J., Brovkin, V., Fraedrich, K., and Wassen, M. J. (2010). Biogeophysical feedbacks trigger shifts in the modelled vegetation-atmosphere system at multiple scales. *Biogeosciences*, 7(4):1237–1245.

Eberle, J. J. and Greenwood, D. R. (2012). Life at the top of the greenhouse eocene world-a review of the eocene flora and vertebrate fauna from canada's high arctic. *GEOLOGICAL SOCIETY OF AMERICA BULLETIN*, 124(1-2):3–23.

Harrington, G. J., Eberle, J., Le-Page, B. A., Dawson, M., and Hutchison, J. H. (2012). Arctic plant diversity in the early eocene greenhouse. *PROCEEDINGS OF THE ROYAL SOCIETY B-BIOLOGICAL SCIENCES*, 279(1733):1515–1521.

Heinemann, M., Jungclaus, J. H., and Marotzke, J. (2009). Warm Paleocene/Eocene climate as simulated in ECHAM5/MPI-OM. *Climate of the Past*, 5:785–802.

Huber, M. and Caballero, R. (2011). The early Eocene equable climate problem revisited. *Climate of the Past*, 7:603–633.

Ilyina, T., Six, K. D., Segschneider, J., Maier-Reimer, E., Li, H., and Nunez-Riboni, I. (2013). Global ocean biogeochemistry model HAMOCC: Model architecture and performance as component of the MPI-Earth System Model in different CMIP5 experimental realizations. *Journal of Advances in Modeling Earth Systems*, 5:287–315.

Janis, C. M. (1993). Tertiary mammal evolution in the context of changing climates, vegetation, and tectonic events. *Annual review of ecology and systematics*, 24:467–500.

Jungclaus, J. H., Fischer, N., Haak, H., Lohmann, K., Marotzke, J., Matei, D., Mikolajewicz, U., Notz, D., and von Storch, J. S. (2013). Characteristics of the ocean simulations in the Max Planck Institute Ocean Model (MPIOM) the ocean component of the MPI-Earth system model. *Journal of Advances in Modeling Earth Systems*, 5(2):422–446.

Kubatzki, C. and Claussen, M. (1998). Simulation of the global bio-geophysical interactions during the last glacial maximum. *Climate dynamics*, 14(7-8):461–471.

Loptson, C. A., Lunt, D. J., and Francis, J. E. (2014). Investigating vegetation-climate feedbacks during the early eocene. *Climate of the past*, 10(2):419–436.

Lorenz, E. (1968). Climatic determinism. *Meteor. Monogr.*, 8:1–3.

Lunt, D. J., Jones, T. D., Heinemann, M., Huber, M., LeGrande, A., Winguth, A., Loptson, C., Marotzke, J., Roberts, C. D., Tindall, J., Valdes, P., and Winguth, C. (2012). A model-data comparison for a multi-model ensemble of early Eocene atmosphere-ocean simulations: EoMIP. *Climate of the Past*, 8(5):1717–1736.

Oyama, M. D. and Nobre, C. A. (2003). A new climate-vegetation equilibrium state for tropical south america. *Geophysical research letters*, 30(23):2199.

Pearson, P., van Dongen, B., Nicholas, C., Pancost, R., and Schouten, S. (2007). Stable warm tropical climate through the eocene epoch. *Geology*, 35(3):211–214.

Pross, J., Contreras, L., Bijl, P. K., Greenwood, D. R., Bohaty, S. M., Schouten, S., Bendle, J. A., Rhl, U., Tauxe, L., Ian Raine, J., Huck, C. E., van de Flierdt, T., Jamieson, S. S. R., Stickley, C. E., van de Schootbrugge, B., Escutia, C., Brinkhuis, H., and Program, I. O. D. (2012). Persistent near-tropical warmth on the antarctic continent during the early eocene epoch. *Nature*, 488:73–77.

Quan, C., Liu, Y., and Utescher, T. (2012). Eocene monsoon prevalence over china: A paleobotanical perspective. *Palaeogeography, palaeoclimatology, palaeoecology*, 365:302–311.

Rachmayani, R., Prange, M., and Schulz, M. (2015). North african vegetation-precipitation feedback in early and mid-holocene climate simulations with ccsm3-dgvm. *Climate of the Past*, 11:175–185.

Reick, C. H., Raddatz, T., Brovkin, V., and Gayler, V. (2013). Representation of natural and anthropogenic land cover change in MPI-ESM. *Journal of Advances in Modeling Earth Systems*, 5(3):459–482.

Renssen, H., Goosse, H., and Fichefet, T. (2003). On the non-linear response of the ocean thermohaline circulation to global deforestation. *Geophysical Research Letter*, 30:1061.

Sluijs, A., Schouten, S., Pagani, M., Woltering, M., Brinkhuis, H., Sinninghe Damste, J. S., Dickens, G. R., Huber, M., Reichart, G., Stein, R., Matthiessen, J., Lourens, L. J., Pedentchouk, N., Backman, J., Moran, K., and the Expedition 302 Scientists (2006). Subtropical Arctic Ocean temperatures during the Palaeocene/Eocene thermal maximum. *Nature*, 441:610–613.

Stevens, B., Giorgetta, M., Esch, M., Mauritsen, T., Crueger, T., Rast, S., Salzmann, M., Schmidt, H., Bader, J., Block, K., Brokopf, R., Fast, I., Kinne, S., Kornblueh, L., Lohmann, U., Pincus, R., Reichler, T., and Roeckner, E. (2013). Atmospheric component of the MPI-M Earth System Model: ECHAM6. *Journal of Advances in Modeling Earth Systems*, 5(2):146–172.

Utescher, T. and Mosbrugger, V. (2007). Eocene vegetation patterns reconstructed from plant diversity - A global perspective. *Palaeogeography Palaeoclimatology Palaeoecology*, 247(3-4):243–271.

Wang, D., Lu, S., Han, S., Sun, X., and Quan, C. (2013). Eocene prevalence of monsoon-like climate over eastern china reflected by hydrological dynamics. *Journal of Asian earth sciences*, 62:776–787.

Wang, G. and Eltahir, E. (2000). Biosphere-atmosphere interactions over West Africa. II: Multiple climate equilibria. *Quarterly journal of the Royal Meteorological Society*, 126(565):1261–1280.

Willis, K. and McElwain, J. (2002). *The elvolution of plants*. Oxford University Press, U.S.A.

Wolfe, J. (1985). Distribution of major vegetation types during the Tertiary. *In: Sundquist E.T., Broecker W.S. (eds) The carbon cycle and atmospheric CO_2: natural variations Archean to present. American Geophysical Union, Washington/DC*, pages 357–375.

Zachos, J., Berza, J., and Wise, S. (1992). Early Oligocene ice-sheet expansion on Antarctica - Stable isotope and sedimentological evidence from Kerguelen Plateau southern Indian-Ocean. *Geology*, 20(6):569–573.

Zachos, J., Pagani, M., Sloan, L., Thomas, E., and Billups, K. (2001). Trends, rhythms, and aberrations in global climate 65 Ma to present. *Science*, 292(5517):686–693.

Zeng, N. and Neelin, D. J. (2000). The role of vegetation-climate interaction and interannual variability in shaping the african savanna. *Journal of Climate*, 13(15):2665–2670.

Table 1. List of Plant Functional Types (PFTs) defined in the land surface scheme JSBACH.

Plant Functional Type
Tropical evergreen trees
Tropical deciduous trees
Extra-tropical evergreen trees
Extra-tropical deciduous trees
Raingreen shrubs
Cold shrubs
C_3 grass
C_4 grass

Table 2. Boundary conditions in the early Eocene climate simulations and in the pre-industrial climate simulations.

	Pre-industrial	Early Eocene
CO_2 concentration	280 ppm	560 ppm
Methane	0.8 ppm	0.8 ppm
Nitrous oxide	0.288 ppm	0.288 ppm
Orbit	pre-industrial	pre-industrial
Bathymetry and orography	present-day	Bice and Marotzke (2001)
Ice sheets	pre-industrial	none

Table 3. Simulations included in the experiment.

	Initial state	Boundary conditions
FP_d	**F**orest world	**P**re-industrial
DP_d	**D**esert world	**P**re-industrial
FE_d	**F**orest world	**E**arly Eocene
DE_d	**D**esert world	**E**arly Eocene
DA_d	Forest world with **d**esert in **A**sia	Early Eocene
FA_d	Desert world with **f**orest in **A**sia	Early Eocene

1
Manuscript prepared for J. Name
with version 2014/09/16 7.15 Copernicus papers of the LaTeX class copernicus.cls.
Date: 23 October 2015

Stability of the Vegetation-Atmosphere System in the Early Eocene Climate

Ulrike Port[1] and Martin Claussen[1,2]

[1]Max Planck Institute for Meteorology, Hamburg D-20146, Germany
[2]Meteorological Institute, University of Hamburg, Hamburg D-20146, Germany

Correspondence to: ulrike.port@mpimet.mpg.de

Abstract. ~~We explore the stability of the atmosphere-vegetation system in the~~ So far, the transitivity of the global system has been analysed for late Quaternary (glacial, interglacial and present-day) climate. Here, we extend this analysis to a warm, almost ice-free ~~early Eocene climate and in the interglacial, pre-industrial climate by analysing the dependence of the system on the initial vegetation cover. The~~ climate with a different configuration of continents. We use the Earth system model of the Max Planck Institute for Meteorology ~~is initialised with~~ to analyse the stability of the climate system under early Eocene and pre-industrial conditions, respectively. We initialise the simulations by prescribing either dense forests or bare deserts on all continents. Starting with desert continents, an extended desert remains in Central Asia in the early Eocene climate. Starting with dense forest coverage, ~~this~~ the Asian desert is much smaller~~because the initially dense vegetation cover enhances water recycling in Central Asia relative to~~, while coastal deserts develop in the Americas which appear to be larger than in the simulations with initially bare continents. These differences can be attributed to differences in the large-scale tropical circulation. With initially forested continents, a stronger dipole in the 200 hPa velocity potential develops than in the simulation with ~~initial deserts. With a smaller Asian desert, the Asian monsoon is stronger than~~ initially bare continents. This difference prevails when vegetation is allowed to adjust to and interact with climate. Further simulations with initial surface conditions that differ in the region of the Asian desert only indicate that local feedback processes are less important in the development of multiple states. In the interglacial, pre-industrial climate, multiple states develop only in the ~~case with a larger desert. The stronger Asian monsoon shifts the global tropical circulation leading to coastal subtropical deserts in North and South America which are significantly larger than with a large Asian desert. This result indicates a global teleconnection of the vegetation cover in several regions. In present-day~~

~~climate, a bi-stability of the atmosphere-vegetation system is found for Northern Africa only . A global teleconnection of bi-stabilities in several regions is absent highlighting that the stability of the vegetation-atmosphere system depends on climatic and tectonic boundary conditions.~~ Sahel region. There, local climate-vegetation interaction seems to dominate.

1 Introduction

The interaction between atmosphere and vegetation may allow for multiple equilibria of the ~~vegetation-atmosphere~~ system pointing to intransitive dynamics in the climate system is as suggested by Lorenz (1968). Multiple equilibrium states have been detected in various model simulations when initialised with different vegetation covers. Claussen (1994), Claussen and Gayler (1997), Claussen (1998), Kubatzki and Claussen (1998), Wang and Eltahir (2000), Zeng and Neelin (2000), and Rachmayani et al. (2015) find multiple ~~state~~ states in Northern Africa, Oyama and Nobre (2003) in the Amazon region, Claussen (1998) in Central Asia, and Dekker et al. (2010) in the northern high latitudes. In all cases, simulations with initially more extended vegetation cover lead to a moister climate and smaller deserts than simulations initialised with sparse vegetation coverage.

~~The~~ Studies which focus on palaeoclimates indicate that the stability of the ~~atmosphere-vegetation~~ climate-vegetation system depends on the climate state. For example, the intransitivity of the ~~atmosphere-vegetation~~ climate-vegetation system over Northern Africa vanishes, or becomes much less pronounced, for the mid-Holocene climate in the simulations by Claussen and Gayler (1997) and Rachmayani et al. (2015), respectively. Likewise, Bathiany et al. (2012) show that the pattern of bi-stability over Northern Africa changes at different times in different ~~location~~ locations during the transition from mid to late Holocene. Such changes in the stability of the ~~atmosphere-vegetation~~ climate-vegetation system may lead to abrupt changes in vegetation and climate due to a loss of stability in the regions which exhibit multiple states (Brovkin et al. 1998; Claussen et al. 1999; Renssen et al. 2003). Further, changes in the stability of the ~~atmosphere-vegetation~~ climate-vegetation system may even induce abrupt changes in locations which seem to be more stable, but which are interlinked with the unstable locations (Bathiany et al. 2013a, Bathiany et al. 2013b).

So far, most studies have assessed the stability of the ~~atmosphere-vegetation~~ climate-vegetation system for interglacial or glacial climate, i.e. ~~a~~ for climate states with permanent ice sheets. Little is known about the transitivity of the ~~atmosphere-vegetation~~ climate-vegetation system in climates that strongly differ from the current late Quaternary climate. Therefore, we explore the stability of the ~~atmosphere-vegetation system in climate of the early Eocene. The~~ climate-vegetation system in a much warmer climate than the present one which does not support permanent ice sheets and sea ice.

During the early Eocene (about 54 to 52 Ma ago) ~~belongs to the warmest periods in the last 65 Million years~~such a warm, almost ice-free climate prevailed. An atmospheric CO_2 concentration

between 300 ppm and 2000 ppm (Beerling and Royer 2011) as well as ~~a different orography and bathymetry than today~~ the specific distribution of continents and bathymetry led to 5°C to 6°C warmer tropics (Pearson et al. 2007) and to mostly ice-free poles (Zachos et al. 1992). The warm climate allowed a dense vegetation cover in almost all regions (Willis and McElwain 2002). Even on Antarctica and in the high North, flora fossils indicate a dense tree cover (Wolfe 1985; Eberle and Greenwood 2012; Harrington et al. 2012; Pross et al. 2012).

~~Using~~ We perform simulations with the Earth system model of the Max Planck Institute for ~~Meteoroloy~~ Meteorology (MPI-ESM) ~~, we simulate~~ and assume continents, bathymetry, and atmospheric CO_2 concentration according to the early Eocene. Other boundary conditions such as orbital parameters, atmospheric methane, and nitrous oxide as well as the assumed plant species in the dynamic vegetation module are the same as in pre-industrial simulations. The resulting simulated climate matches temperature reconstructions of the early Eocene fairly well. Only in the high latitudes, the simulated near-surface temperature is lower than reconstructions suggest. Despite this mismatch, the simulated Eocene-like climate fulfills our demand because we rather aim to investigate the stability of the climate-vegetation system in a warm almost ice-free climate than to reproduce the climate of the early Eocene ~~climate and~~ as well as possible.

To compare the stability of the climate-vegetation system in the warm Eocene-like climate and in the pre-industrial climate~~. We start simulations from two~~ , we perform the same experiment with boundary conditions for both these climates. The respective experiments contain two simulations each which start from different vegetation states~~, all~~ : All ice-free continents are either completely covered with dense forests or with bare-soil deserts, respectively~~()~~. From these initial states, the model system is allowed to freely evolve, with dynamically interacting atmosphere, ocean, and vegetation. Depending on the initial conditions, new equilibria in the ~~vegetation-atmosphere~~ climate-vegetation system are reached after some 1000 years of simulation.

2 Experiment

2.1 Model

The Earth system model of the Max Planck Institute for Meteorology (MPI-ESM) consists of the atmospheric general circulation model ECHAM6 (Stevens et al. 2013), the Max Planck Institute Ocean Model MPIOM (Jungclaus et al. 2013), the land surface scheme JSBACH (Reick et al. 2013), and the ocean biogeochemistry model HAMOCC (Ilyina et al. 2013). We use ECHAM6 in a horizontal resolution is T31 (approximately 3.75°) and with 31 levels in the vertical. The ocean grid has a horizontal resolution of about 3° and 40 levels in depth.

JSBACH includes a dynamic vegetation module based on a tiling approach (Brovkin et al. 2009). Vegetation is represented by eight Plant Functional Types (PFTs) which reflect present-day plant taxa (Tab. 1). ~~During the early Eocene, however, plant types have been differed from today. Grass~~

land is common today, but it did not exist during the early Eocene (). C_3 spreaded in the early to mid Miocene (20 - 10 Ma) (), while C_4 expanded during the mid to late Miocene (). Instead, other plant species dominated the vegetation cover during the early Eocene which are extinct, or almost extinct, today such as paratropical rainforest or polar forest (). In our study, we neglect any differences in plant taxa. Thus, we focus on the biogeophysical processes and their differences between early Eocene and pre-industrial climate. The effect of difference between early Eocene and current plant taxa will be the focus of subsequent studies.

2.2 Early Eocene setting

For our early Eocene simulations, we We perform the same simulations for an interglacial climate and a warm ice-free climate. To get an interglacial climate, we assume pre-industrial boundary conditions for the chemical composition of the atmosphere, orbital parameters, continents, orography, and bathymetry (Tab. 3). To achieve a warm ice-free climate, we use the same boundary conditions as . Orography and bathymetry are based on the boundary conditions which Heinemann et al. (2009) use for their Eocene simulation. Like they do, we prescribe the orography and bathymetry maps by Bice and Marotzke (2001)which interpolated from the original resolution of 2° times 2° to the model resolution of T31. The orography map lacks information on sub-grid orography such as slope, anisotropy, orientation, standard deviation, maxiumummaximum, minimum, and mean elevation. Without these informationsinformation, sub-grid interactions of atmospheric flow with orography can not be parameterised in ECHAM6 (Stevens et al. 2013). Hence, we turn off the module for sub-grid orographic drag and wave generation.

In the standard version of MPIOM, the grid poles are over Greenland and Antarctica. With Eocene continents, the pole over present-day Greenland coincide with the Palaeo-Atlanic Palaeo-Atlantic Ocean, i.e. meridians converge at this pole leading to numerical singularitiessingularities. To avoid singularitiessingularities, we use the setting by Heinemann et al. (2009) who placed the MPIOM north pole and south pole to the large continents of Palaeo-Asia and to Palaeo-South America, respectively.

The atmospheric CO_2 concentration is fixed to 560 ppm (Tab. 2), which is the lower limit of reconstructions (). Methane Zachos et al. 2001 and Beerling and Royer 2011). With a fixed atmospheric CO_2 concentration, carbon pools does not need to reach an equilibrium which would take several thousand year. Instead, living biomass responses to a constant atmospheric CO_2 and equilibrates already after several decades. Since our simulations run for 1000 years, this time span is long enough to reach an equilibrium in living biomass.

The other greenhouse gases methane and nitrous oxide are set to pre-industrial values in the early Eocene atmosphere and also the orbit corresponds to the pre-industrial orbit (Tab. 2). This approach limits the differences between Soil properties are the same as in the pre-industrial simulations and represent clay. Soil dynamics are not considered, i.e. soils remain constant over the whole simulations.

During the early Eoceneand the pre-industrial boundary conditions to the distribution of continents, the bathymetry, the presence of ice sheets, and the atmospheric CO_2 concentration, plant species have been differed from today. For instance, grass land is common today, but evolved after the early Eocene (Willis and McElwain 2002). C_3 spread in the early to mid Miocene (20 - 10 Ma) (Janis 1993), while C_4 expanded during the mid to late Miocene (Cerling et al. 1993). Instead, other plant species dominated the vegetation cover during the early Eocene which are extinct, or almost extinct, today such as paratropical rainforest or polar forest (Wolfe 1985). We neglect any differences in plant taxa to isolate the geographic and climatic factors affecting the stability of the climate-vegetation system.

To initialise our Eocene simulations, we perform a simulation starting from the equilibrium Eocene climate by Heinemann et al. (2009). Like in their simulation, we assume a savannah vegetation with a desert cover of 40 %, a tree cover of 24 %, and a grass cover of 36%. After 300 years, near-surface temperature and upper-level ocean temperatures are in equilibrium. Only in the deep ocean, a marginal temperature trend remains.

2.2 Simulations

Our simulationsstart from the simulations by . They explore the impact of extreme land cover on the early Eocene climate and the pre-industrial climate by simulating and a 'desert world' and a 'forest world' for both climates, respectively

Starting from the equilibrium Eocene climate, we perform two simulations. In the 'desert world', no vegetation occurs on all continents during the simulated first 400 years. In the 'forest world ', trees cover all ice-free continents completelyyears of the simulations, vegetation is fixed to dense forest in the FE_f simulation and to bare soil in the DE_f simulation. After that period, the forest world and desert world simulation continue with a dynamically evolving vegetation cover in the FE_d simulation and in the DE_d simulation, respectively.

In order to separate the albedo effect of vegetation from the hydrological effect, simulate the forest world and the desert world we perform the initial desert simulation and the initial forest simulation two times, respectively. All soils either have a homogeneous albedo of 0.1 (dark soil) or 0.4 (bright soil). In the dark soil case, soil and vegetation have about the same albedo leading to weak albedo changes by vegetation relative to bare soil. In other words, vegetation affects climate mainly through the hydrological cycle. In the bright soil case, vegetation has a much lower albedo than soil. Hence, both, the albedo effect and the hydrological effect of vegetation are pronounced.

At the end of the simulations by , climate differs significantly between the forest worlds and the desert worlds. We extend those simulations by further 1000 years. During the extended simulations, atmosphere, ocean, and vegetation interact and thus, vegetation establishes, migrates, and retreats dynamicallyact. In the bright-soil simulations, the vegetation-atmosphere climate-vegetation system reaches the same state when initialised with dense forest as when initialised with bare soil. As we

focus on intransitive dynamics in the ~~vegetation-atmosphere~~ climate-vegetation system, we exclude a detailed discussion of the bright-soil simulations in this study. Instead, we present the results for the dark-soil simulations where multiple equilibria establish depending on the initial vegetation cover in ~~both, the early Eocene and the pre-industrial~~ the warm ice-free climate. Table 3 gives an overview of the considered four simulations where all soils have a low soil albedo.

3 ~~Results and Discussion~~

2.1 ~~Early Eocene climate~~

~~The warm and humid early Eocene climate favours dense vegetation cover in almost all regions. Only~~ To analyse the local impact of initial vegetation cover on the intransitivity, we perform two additional simulations with Eocene boundary conditions. In the DA_f simulation, we fix the vegetation cover to bare soil in Central Asia and ~~in southern Africa, deserts remain in the DE simulation(Fig. ??). Subtropical semi-deserts establish in South America, North America, and Australia. In these arid and semi-arid regions, pronounced differences in vegetation cover emerges between the DE simulationand the FE simulation(Fig. 3).~~ to forests elsewhere and simulate 400 years. Starting from the DA_f simulation, we let the vegetation evolve dynamically in the DA_d simulation. Analogously, we assume a dense forest in Central Asia and deserts elsewhere in the FA_f simulation. After 400 years with a fixed vegetation cover, vegetation evolves dynamically in the FA_d simulation.

~~Desert cover in the DE simulation. The average over the last 30 years of the simulation is shown. Green indicates a minimum desert cover. Blue refers to semi-desert conditions. Yellow marks desert regions.~~ Analogue to the Eocene simulations, we perform two pre-industrial simulations. The FP_f simulation runs for 400 years with a fixed forest cover on all ice-free continents. Afterwards, vegetation establishes dynamically in the FP_d simulation. In the DP_f simulation, vegetation is fixed to desert for 400 years. Starting from the DP_f simulation, vegetation evolves dynamically in the DP_d simulation.

3 Warm almost ice-free climate and its vegetation cover

~~Differences in vegetation cover between the simulations that start from a forest world and the simulations that start from a desert world. Shown are differences for the early Eocene climate (FE - DE) (a) and for the pre-industrial climate (FP - DP) (b). Mapped differences refer to the average over 30 years and are significant on a 95level. Woody types include all trees and shrubs. Grass types refer to C_4 grass and to C_3 grass. Green colours indicate a higher cover fraction in the FD than in the DD simulation. Purple colours refer to a smaller cover fraction in the FD simulation. Black contour lines mark regions which are analysed in more detail in Fig. 4 and Fig. 9.~~ Near-surface temperature in the DE_d simulation agrees with temperature reonstructions of the early Eocene temperature in the topics and subtropics. In the northern mid to high latitudes, the DE_d simulation

is colder than reconstructions of Eocene temperatures (Fig. 1). Relative to the TEX_{86} estimate by ? north of Greenland, the simulated sea-surface temperature (SST) is even 18 K lower. The TEX_{86} estimate, however, likely represents summer temperatures (?). Considering summer values, the DE_d simulation is 15 K colder than temperature estimates suggest for the early Eocene.

~~In the semi-desert in western North America (marked in Fig. 3), the desert cover is larger by 0.43 in the FE simulation than in the DE simulation and precipitation is smaller by 0.52 mm/day (70)~~ In the southern high latitudes, the simulation agrees with marine and terrestrial temperature estimates. The only exception is the SST reconstruction by ? that suggests temperature of 24°C at the Tasman Plateau (Fig. ~~4 c). In the semi-desert in southern South America, desert cover is larger by 0.19 and precipitation is smaller by 0.5 mm/day (43~~1). Like the estimate by ?, the estimate by ? is based on TEX_{86} and likely has a bias to summer temperatures. Considering the summer temperature, our simulation is colder than the reconstruction by 9 K over the southern Pacific Ocean.

Despite the mismatch of our simulated early Eocene climate with reconstructions in the high latitudes, the simulation fullfills our demands for a warm ice-free climate. At the end of the DE_d simulation, global mean temperature is 7.1 K higher than at the end of the pre-industrial DP_d simulation. The temperature difference is most pronounced in the high latitudes where the DE_d climate is warmer than the DP_d climate by 34.5 K south of 70°S and 10.3 K north of 70°. In the tropics, the temperature difference is 5.4 K leading to a weaker pole-to-equator temperature gradient in the DE_d climate than in the DP_d climate. With above freezing temperatures during most time of the year even in the high latitudes, permanent ice is absent and sea ice occurs only seasonally in the Arctic Ocean. The hydrological cycle is enhanced in the DE_d climate with 15 % ~~) in the FE simulation (Fig. 4 b). The differences on the American continents are counterintuitive because starting from dense forest leads to a larger desert in these regions than starting from bare soil. This result disagrees with all simulations previously mentioned in the introduction. Later, we will discuss the mechanism causing these bi-stabilities~~stronger precipitation than in the DP_d climate.

~~In the semi-desert in southern Africa (marked in Fig. 3), desert cover is smaller by 0.12 at the end of the FE simulation than~~

In the warm and humid Eocene-like climate, MPI-ESM simulates a dense vegetation cover which matches vegetation reconstructions in the high latitudes (Fig. 2). Like the flora fossil assemblage by Utescher and Mosbrugger (2007) suggests, extra-tropical trees cover Antarctica and reach the Arctic Ocean in the High North at the end of the DE~~simulation (Fig. 4 d). However, considering the trend of -0.04 and 0.07 per 100 years at the end of the FE and DE simulation~~$_d$ simulation. Beside trees, our model simulates plenty C_3 grass in the mid to high latitudes. The grass cover disagrees with reconstruction because wide-spread grassland likely evolved after the early Eocene, between the late Eocene (?) and the early to mid Miocene (20-10 Ma) (Janis 1993). C_3 grass is a common PFT in JSBACH and we decided to stay with it despite the discrepancy to the Eocene plant taxa. This approach excludes the influence of characteristic Eocene plant taxa on the stability

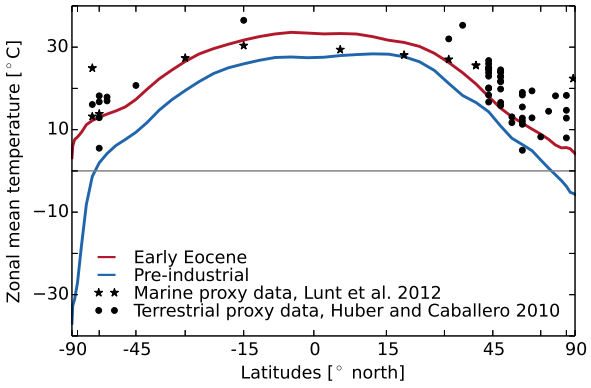

Figure 1. Zonal annual mean 2-m temperature in the DE_d simulation (red line) and in the DP_d simulation (blue line). Stars show estimates of annual-mean sea-surface temperature (SST) and near-surface temperature for the early Eocene based on $\delta^{18}O$, Mg/Ca, and TEX_{86} (**?**). Cycles refer to terrestrial annual mean temperature estimates based on macrofloral and palynoflora assemblage data and from teeth, hydrogen isotopes, and oxygen isotopes (**?**).

of the climate-vegetation system and reveals the sensitivity of the stability to geophysical boundary conditions (continents, bathymetry, and atmospheric CO_2).

Tropical forest is bounded between 30°S and 30°N in the DE_d simulation but reconstructions suggest a poleward extent up to 60°S and 60°N during the early Eocene (Fig. 2) (Wolfe 1985, ~~the difference in vegetation cover may not be significant~~Willis and McElwain 2002, Utescher and Mosbrugger 2007) . We assume that the mismatch results from the cold bias in the simulated high latitude temperature discussed above. C_4 grass coexist with tropical forest in the tropics in the DE_d simulation, but the C_4 pathway evolved and expanded during the late Miocene (Cerling et al. 1993). Like for C_3 grass, we decided to stay with C_4 grass to limit the difference between the Eocene simulations and the pre-industrial simulations to differences in continents, bathymetry, and atmospheric CO_2.

~~Time series of desert cover and precipitation in selected regions in Central Asia (a), South America (b), North America (c), and Africa (d) in the FE simulation (green line) and in the DE simulation (orange line). The regions are marked in Fig. 3. Both time series show five-year mean values.~~

~~In~~ In general, deserts are suggested to have been rare in the warm climate of the early Eocene (Willis and McElwain 2002). Only in Central Asia, sediments and flora fossils indicate semi-dry to dry conditions with desert vegetation (**?** and **?**). Like previous simulations by **?** and **?**, our simulation reproduces the Asian desert ~~, the differences in~~ because a monsoon climate causes a seasonally dry climate in this region. In subtropical Africa and America, further small deserts and semi-desert evolve in the DE_d simulation.

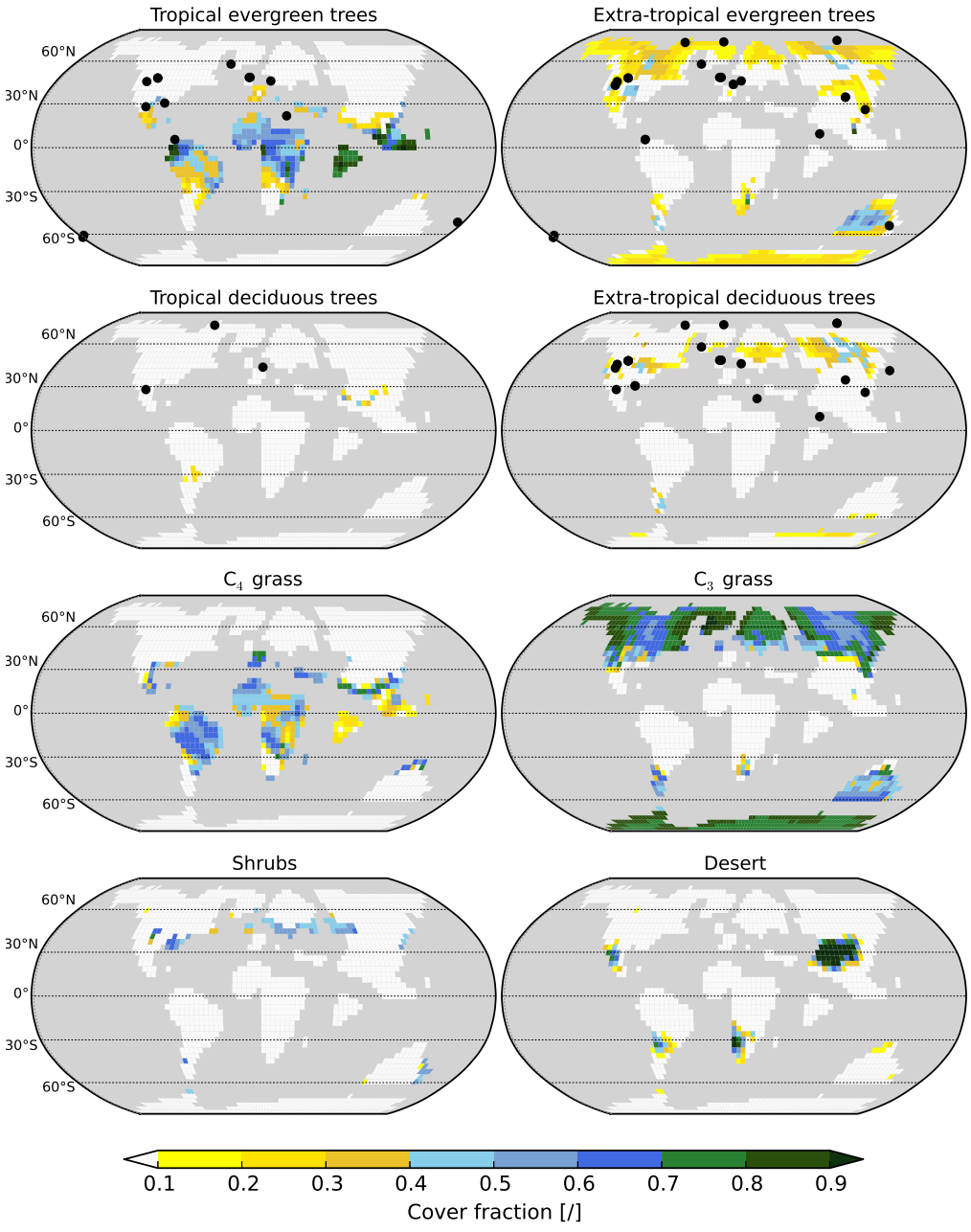

Figure 2. Simulated vegetation cover in the DE_d simulation and reconstructed vegetation based on the flora collection by Utescher and Mosbrugger (2007). Locations are marked where the diversity of the respective PFT in flora collection exceeds 10%.

4 Results and Discussion

4.1 Bi-Stable deserts in the Eocene climate

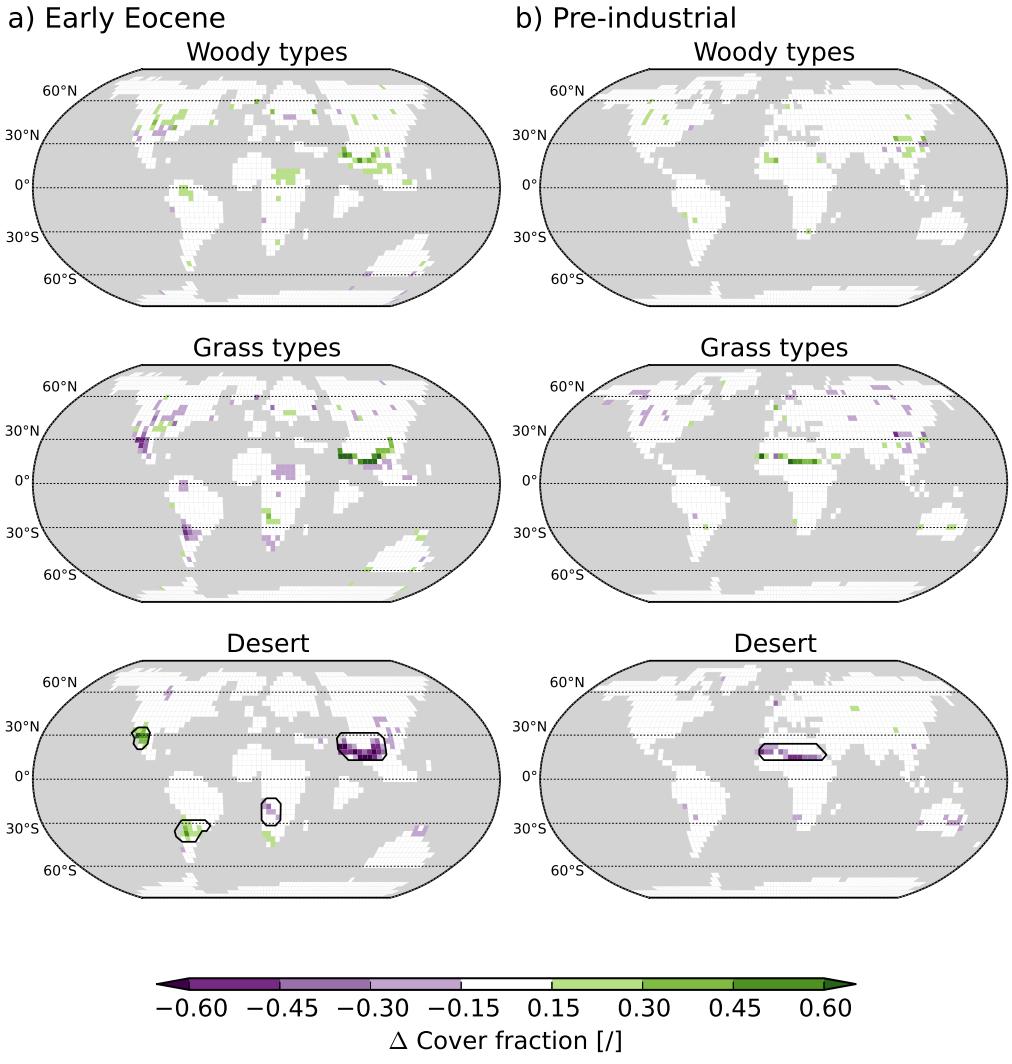

Figure 3. Differences in vegetation cover between the simulations that start from a forest world and the simulations that start from a desert world. Shown are differences for the early Eocene climate (FE_d - DE_d) (a) and for the pre-industrial climate (FP_d - DP_d) (b). Mapped differences refer to the average over 30 years and are significant on a 95% level. Woody types include all trees and shrubs. Grass types refer to C_4 grass and to C_3 grass. Black contour lines mark regions which are analysed in more detail in Fig. 4 and Fig. 9.

The warm and humid early Eocene climate favours a dense vegetation cover in almost all regions. Only in Central Asia and in southern Africa, deserts remain in the DE_d simulation (Fig. 2), and subtropical semi-deserts establish in South America, North America, and Australia. In these arid and semi-arid regions, pronounced differences in vegetation cover emerge between the DE_d simulation and the FE_d simulation (Fig. 3).

The difference in the vegetation cover ~~are most pronounced~~ is most pronounced in the Asian desert (region marked in Fig. 3). At the southern edge of the desert, more grass and trees remain in the FE_d simulation than in the DE~~simulation (Fig. 3)~~$_d$ simulation because precipitation is stronger. At the ~~beginning~~ end of the FE~~simulation, the dense forest transpires 1.35 mm/day leading to an evapotranspiration of 1.7 mm/day and a precipitation of 1.8 mm/day~~ $_d$ simulation, precipitation in Central Asia is 1.58 mm/day stronger and desert cover is 0.36 smaller (Fig. 4 a). ~~During the FE simulation, precipitation is sufficient to maintain a large part of the vegetation cover which preserves high transpiration rates and strong precipitation. By~~ Also in the semi-desert in southern Africa, desert cover is smaller at the end of the FE~~simulation, desert cover amounts to 0.43 and precipitation to 0.82 mm/day in Central Asia.~~

~~At the beginning of the DE simulation, evapotranspiration in Central Asia is ten times weaker~~ $_d$ simulation than at the ~~beginning of the FE simulation and precipitation is six times smaller~~ end of the DE_d simulation (Fig. 4 ~~a). Starting from this dry climate, only little vegetation establishes preserving a dry climate in Central Asia. At~~ d).

In the semi-desert in western North America, precipitation is smaller by 0.52 mm/day (70%) at the end of the FE_d simulation than at the end of the DE~~simulation~~$_d$ simulation. In the drier climate, desert cover ~~in Central Asia~~ is larger by ~~0.36 than in the FE simulation and precipitation weaker by 0.6 mm/day.~~

~~In both,~~ 0.43 (Fig. 4 c). Also in the semi-desert in southern South America, a weaker precipitation in the FE_d simulation results in a larger desert cover than in the ~~FE and the DE simulation , soil have an albedo of 0.1 which is similar to the albedo of vegetation. Hence, the albedo effect of vegetation is weak and the multiple stable vegetation-atmosphere states in Central Asia result from a hydrological feedback. As vegetation increases precipitation in Central Asia mostly during the Asian monsoon~~ DE_d simulation (Fig. ~~??~~), ~~we suggest that vegetation enhances water recycling leading a stronger Asian monsoon and to more precipitation relative to bare soil and feeding back to vegetation growth.~~

~~Above, we show that the semi-deserts~~ 4 b). The differences on the American continents are ~~larger in the simulation with initial forest cover than in the simulation with initial desert.~~ counterintuitive because starting from dense forest leads to a larger desert in these regions than starting from bare soil. This result disagrees with all simulations previously mentioned in the introduction. Later, we will discuss the mechanism causing these bi-stabilities.

To identify the driving ~~mechanism for this bi-stability~~mechanisms for the multiple steady vegetation states, we analyse the ~~impact of vegetation on the large scale atmospheric circulationin further detail~~large-scale atmospheric circulation. Following Claussen (1997), we compute the velocity potential at 200 hPa which is an indicator of ~~large scale,~~ large-scale upper-air divergence and convergence, and hence, convection and subsidence in the tropics. The separation of the horizontal wind, $\boldsymbol{V}$, in the rotational component, $\boldsymbol{V}_\Psi$, and in the divergent component, $\boldsymbol{V}_\chi$, yields

$$\boldsymbol{V} = \boldsymbol{V}_\Psi + \boldsymbol{V}_\chi. \tag{1}$$

The divergent part of the horizontal wind is the gradient of the velocity potential, χ,

$$\boldsymbol{\nabla}\chi = \boldsymbol{V}_\chi. \tag{2}$$

~~Annual cycle of precipitation in early Eocene Central Asia. The respective region is marked in Fig. 3. Lines refer to the FE simulation (green) and the DE simulation (orange). The average over the last 30 years of each simulation is considered.~~

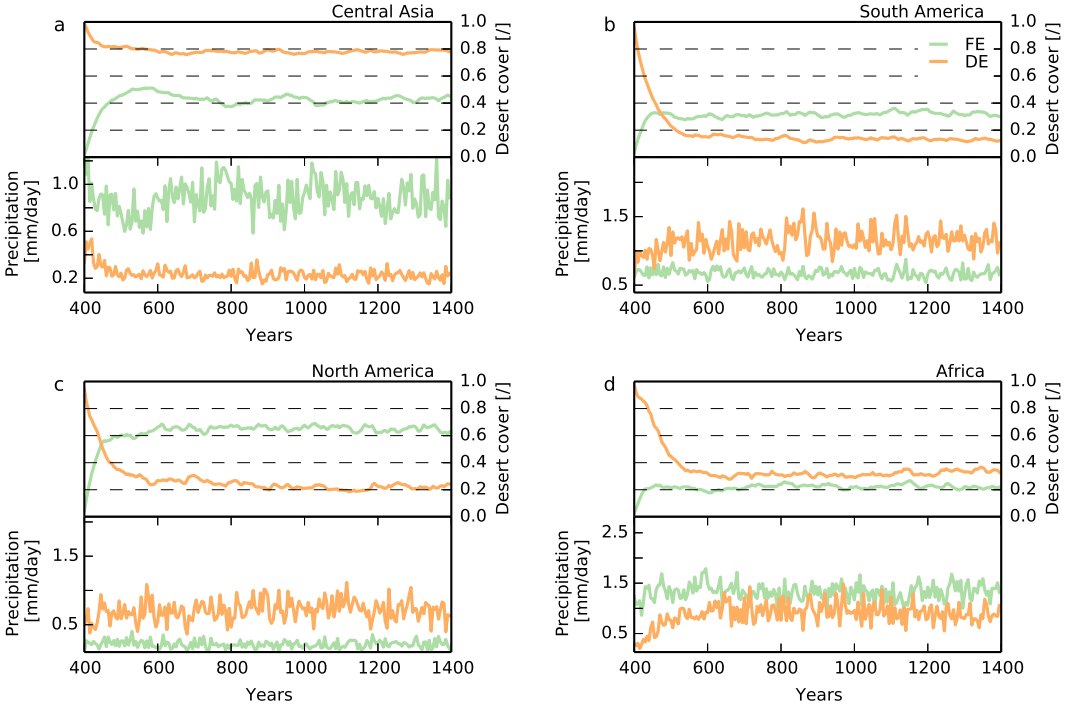

Figure 4. Time series of five-year mean desert cover and precipitation in selected regions in Central Asia (a), South America (b), North America (c), and Africa (d) in the FE_d simulation (green line) and in the DE_d simulation (orange line). The regions are marked in Fig. 3.

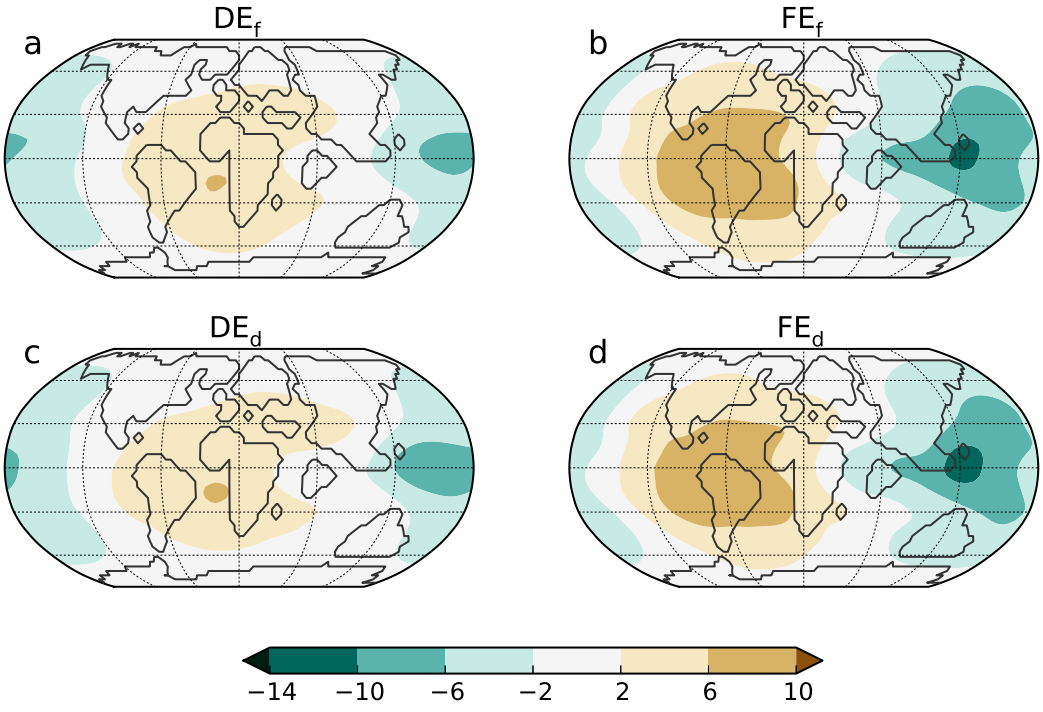

Figure 5. Velocity potential at 200 hPa ~~in~~ at the ~~DE~~ end of the desert world simulation (a), forest world simulation (b), DE$_d$ simulation (c), and ~~in the~~ FE$_d$ simulation (~~b~~d). The average over the last 30 years of the ~~simulations~~ respective simulation is ~~shown~~considered. The DE$_d$ simulation and the FE$_d$ simulation start from the desert world simulation and the forest world simulation, respectively. Brown colours indicate to a positive velocity potential, upper-air convergence, and subsidence. Green colours indicate to a negative velocity potential, upper-air divergence, and rising.

Hence, the divergent part of the ~~large scale~~ large-scale horizontal wind is directed towards the strongest increase in the velocity potential. This relation implies that air flows from the centre of negative velocity potential to the centre of positive velocity potential. Therefore, upper air diverges in the centre of negative velocity potential and converges in the centre of positive velocity potential. Below the divergence, air rises and below the convergence, air subsides.

~~Figure 5 a) shows a bipolar pattern in~~

Figure 5 shows the velocity potential in the desert world, DE$_f$, and in the forest world, FE$_f$, at 200 hPa ~~at the end of the DE simulation. The~~ averaged over the last 30 years of the simulations. In the desert world, the centre of positive velocity potential indicates strong subsidence over the tropical Atlantic Ocean, ~~while~~ and the centre of negative velocity potential implies convection over the ~~western Pacific Ocean . Over Central Asia, positive velocity potential prevails indicating subsidence over this region.~~ tropical Pacific Ocean (Fig. 5 a). In the forest world, the centre of subsidence intensifies

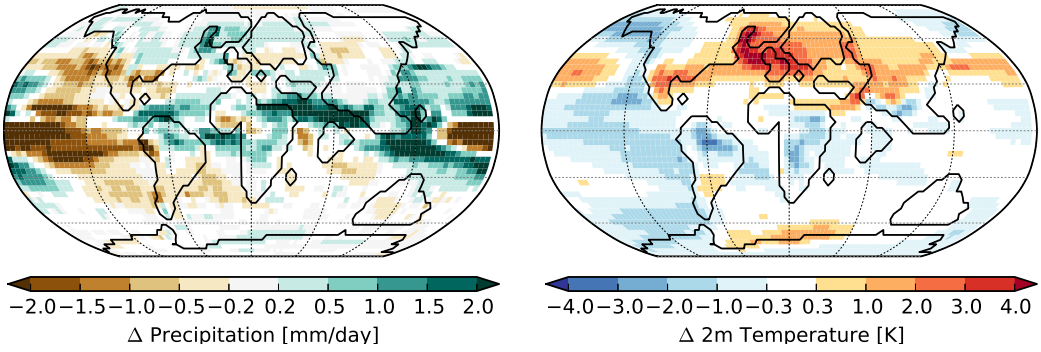

Figure 6. Differences in precipitation and 2-m temperature between the FE_d simulation and the DE_d simulation. The average over the last 30 years of the simulations is considered. Depicted differences are significant on a 95% level.

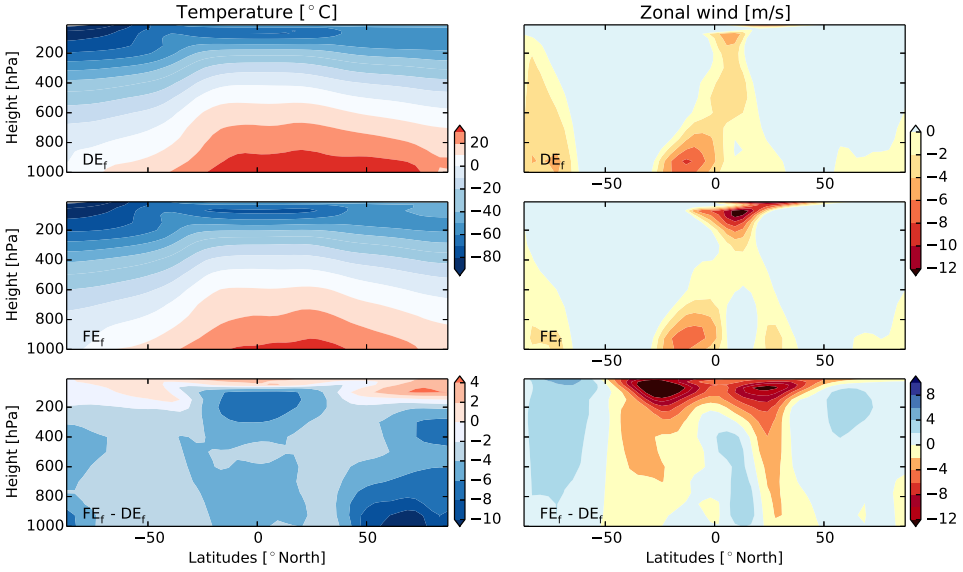

Figure 7. Zonal-mean temperature and wind in the desert world simulation, DE_f, and in the forest world, FE_f, simulation of the early Eocene climate. Further, the differences between the forest world simulation and the desert world simulation (FE_f - DE_f) is shown. The average over July and August in the last 30 years of the simulations is considered.

and shifts to northern South America relative to the circulation in the desert world, and the centre of convection intensifies and shifts to the western Pacific Ocean (Fig. 5 b).

~~In the FE simulation, velocity potential pattern differs from the DEsimulation~~

Starting from the desert world simulation and the forest world simulation, vegetation cover evolves dynamically with climate during the DE_d simulation and the FE_d simulation, respectively. The

initial large-scale atmospheric circulation pattern, however, persists (Fig. 5 ~~b). In Central Asia more vegetation remains in the FE simulation than in the DEsimulation. The additional vegetation enhances convection over this region as indicated by the negative velocity potential. With a~~ c, d). Hence, at the end of the simulations, the atmospheric circulation still differs strongly between the DE_d simulation and the FE_d simulation. With stronger convection over ~~Asia, the amplitude of the velocity potential pattern increases and the pattern shifts westwards~~ the west Pacific Ocean in the FE_d simulation, precipitation at the southern edge of the Asian desert is stronger than in the DE_d simulation leading a smaller desert cover. Over the American continents where subsidence strengthens relative to the DE~~simulation indicating different large scale atmospheric circulations in both simulations~~$_d$ simulation, the subtropical semi-arid regions are drier, and desert cover is larger.

~~With a different global atmospheric circulation, precipitation differs significantly between the FE and the DE simulation~~ In the desert world, a temperature gradient occurs above 100 hPa between cold air above the tropics and warmer air above the mid and high latitudes (Fig. ~~6). At the west coast of the American continents, precipitation is weaker in the FE simulation leading to less vegetation in the semi-arid regions in western North America and southern South America. In other words, the multiple vegetation-atmosphere states in these semi-arid regions seem to be connected to the multiple vegetation-atmosphere states in Central Asia~~7). This meridional temperature gradient induces a weak easterly wind at about 5°N due to the thermal wind relation (Fig. 7). In the forest world, near-surface temperature is reduced relative to the desert world, and in the colder climate, tropopause is lower leading to a warming at the tropopause. The tropopause decline and the connected the warming reach 200 hPa in the mid and high latitudes and 100 hPa in the tropics. Due to the weaker warming in the tropics than in the mid to high latitudes, the meridional temperature gradient between tropics and mid to high latitudes enhances relative to the desert world. With a stronger meridional temperature gradient, the easterly wind at 100 hPa strengthens in the forest world.

~~Such a connection of multiple vegetation states in several regions, so far, has not been found for the present-day climate. simulates a shift in the atmospheric circulation with different vegetation states in the Sahara. However, the shifted atmospheric circulation affects the vegetation in~~ The stronger easterly wind in the ~~Sahara only.~~ forest world transports more air from the convection zone over Asia to the subsidence zone over America than in the desert world. The enhanced air transport manifests in an intensified velocity potential pattern and a general westward shift relative to the desert world (Fig. 5). This result suggests that forest affects large-scale atmospheric circulation by reducing near-surface temperature, lowering tropopause height, and thereby, enhancing the easterly wind at the tropopause.

~~Precipitation differences between the FE simulation and the DE simulation. The average over the last 30 years of the respective simulation is considered. Depicted differences are significant on a 95level.~~ During the FE_d simulation, the warming in the height becomes weaker but the easterly wind is still stronger than in the DE_d simulation and supports the intensified and shifted velocity potential

pattern (not shown here). The persistence of the stronger easterly wind in the FE_d simulation again indicates that the initial forest cover shifts the atmospheric circulation to another self-preserving state than the desert cover.

~~The question remains which mechanism links the multiple stable vegetation states~~ To test whether large-scale or local initial vegetation causes the bi-stability in the climate-vegetation system, we perform two additional simulations. In the Asian Desert simulation, DA_f, we fix the vegetation cover to a desert in Central Asia ~~and on the American continents. Both regions are connected through the Walker circulation. In the present-day climate, the Walker circulation describes the zonal atmospheric circulation over the subtropical Pacific Ocean. In combination with the zonal ocean circulation in the Pacific Ocean, the Walker circulation forms the El Niño-Southern Oscillation.~~ (marked region in Fig. 8) and to forests elsewhere and simulate 400 years. After that, we let the vegetation evolve dynamically during the DA_d simulation. Analogously, we assume a dense forest in Central Asia and deserts elsewhere in the Asian Forest simulation, FA_f. After 400 years with a fixed vegetation cover, vegetation evolves dynamically in the FA_d simulation.

~~In the early Eocene simulations, the strong bipolar pattern in the velocity potential is associated with a zonal circulation similar to the tropical Walker circulation today: Air rises over the western Pacific Ocean and subsides over the eastern Pacific Ocean (Fig. 5). In the FE simulation , this bipolar pattern is more pronounced indicating that vegetation in central Asia enhances the convection branch of the Walker circulation relative to the DEsimulation. Due to continuity reasons, stronger convection in Asia causes stronger subsidence over the American continents and, therefore, less vegetation in the American subtropics~~

In the DA_f simulation, when vegetation is fixed, the atmospheric circulation reaches the same state as in the forest world. Then, vegetation evolves dynamically and the circulation pattern persists ending up in the same stable state as in the FE_d simulation. Analogously, the FA_f simulation yields the same large-scale atmospheric circulation as the desert world simulation. With a dynamically evolving vegetation cover, the atmospheric circulation persists leading to the same state in the FA_d simulation as in the DE_d simulation. The agreement of the DA_d simulation with the FE_d simulation and the FA_d simulation with the DE_d simulation shows that local initial vegetation fails to cause multiple climate-vegetation states. Instead, our results suggest that large-scale initial vegetation cover causes multipe climate-vegetation states in the warm, ice-free climate.

4.2 ~~Pre-industrial~~ Bi-stable Sahel in the pre-industrial climate

In the pre-industrial ~~Sahel, more vegetation remains in the FPsimulation than establishes in the DPsimulation (marked region in Fig. 3). Time series of desert cover and precipitation in the Sahel illustrate that~~ climate, the vegetation difference between the FP_d simulation and the DP_d simulation is restricted to the Sahel. More vegetation remains in this region and the desert cover is smaller by 0.21 ~~at the end of the FPsimulation than at the end of the DPsimulation and~~ in the FP_d simulation

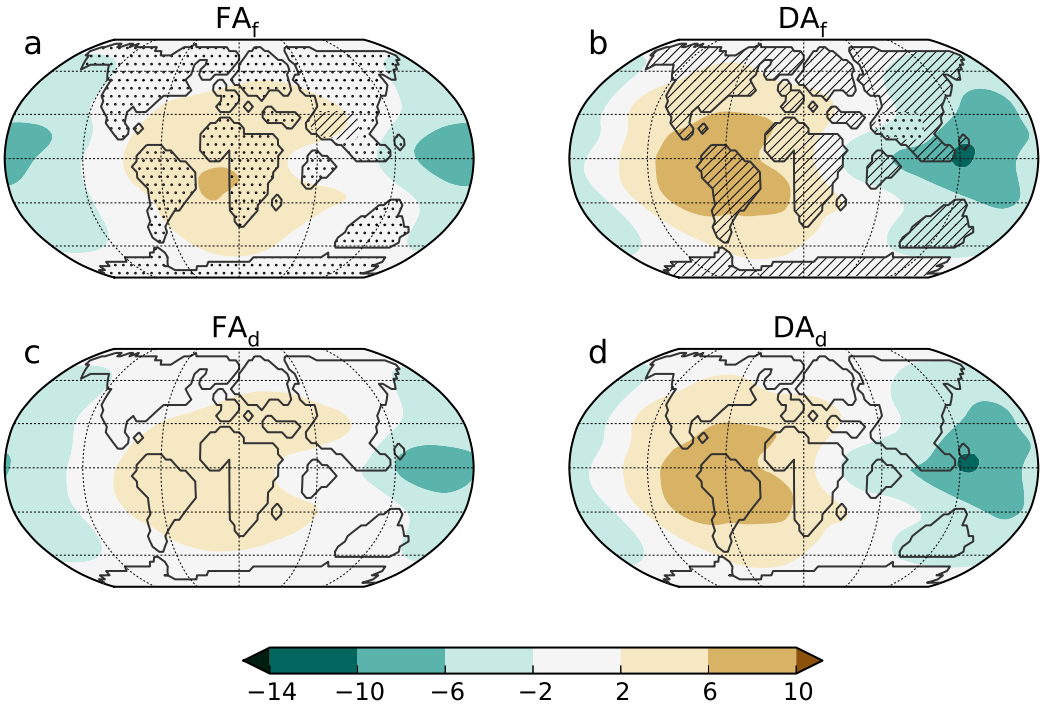

Figure 8. Velocity potential at 200 hPa at the end of the FA$_f$ simulation and DA$_f$ simulation (a-b), and at the end of the FA$_d$ simulation and DA$_d$ simulation (c-d). The average over the last 30 years of the respective simulation is considered. Brown colours indicate to a positive velocity potential, upper-air convergence, and subsidence. Green colours indicate to a negative velocity potential, upper-air divergence, and rising.

than in the DP$_d$ simulation. Consistently, precipitation is about two times ~~stronger~~ larger in the FP$_d$ simulation than in the DP$_d$ simulation (Fig. ~~9~~11).

~~In comparison to the stability of the vegetation-atmosphere system in the early Eocene climate, only the vegetation in the Sahel is bistable indicating that globally connected bi-stabilties in several regions are absent in the~~

In contrast to the Eocene simulations, the large-scale atmospheric circulation, as indicated by the 200 hPa velocity potential, differs only slightly between the forest world simulation and the desert world simulation for pre-industrial ~~climate. To identify the reason for the different stability of the vegetation-atmosphere system in the early Eocene and~~ climate (Fig. 10 a, b). When vegetation is allowed to dynamically adjust to and to interact with climate, the small differences in the large-scale atmospheric circulation between the initially forested world and the initially deserted world nearly vanish (Fig. 10 c, d). The weak impact of initial vegetation on the large-scale atmospheric circulation implies that a local effect rather than a large-scale effect leads to multiple climate-vegetation states in the pre-industrial ~~climate, we analyse the velocity potential at 200 hPa in Figure 10. The positive~~

velocity potential over the Sahel implies that subsidence prevails over this region. Even the additional vegetation Sahel climate.

In the Sahel, evapotranspiration amounts to 1.1 mm/day in the FP_d simulation and 0.64 mm/day in the DP_d simulation. Cloud cover is larger, less solar radiation reaches the surface and latent heat flux is larger by a factor of 1.7 in the FP_d simulation than in the DP_d simulation. Consistently, a stronger meridional temperature gradient develops with warmer air over the Sahara and colder air over the Sahel in the FPsimulation does not enhance convection. Presumably, the subsidence over the Sahel prevents vegetation from inducing strong convection.

As vegetation fails to enhance convection over the Sahel , the global atmospheric circulation is almost the same d simulation than in the DP_d simulation (Fig. 11). The increased temperature gradient enhances the African Easterly Jet (AEJ) at 700 hPa in the FP_d simulation (Fig. 12). Stronger AEJ over moister or greener Sahel region is in line with earlier simulations by **?** and Rachmayani et al. (2015), respectively. The stronger AEJ is accompanied with a stronger horizontal moisture flux convergence (Fig. 12) which, in turns leads to larger precipitation over the Sahel in the FPsimulation and the DP simulation leading to only weak differences in precipitation between both simulations d simulation than in the DPd simulation (Fig. 11). Especially outside Northern Africa and over continents, precipitation differences are

In the studies by Claussen and Gayler (1997) and Claussen (1998), strong differences in surface albedo triggered multiple stable vegetation–atmosphere states in the Sahara and Sahel. In our study, albedo differences are assumed to be small. Hence, further multiple stable vegetation states in other regions than Northern Africa are absent.a hydrological feedback causes multiple states as it is the case in the simulations by Rachmayani et al. (2015).

In short, the large scale atmospheric circulation limits the multiple stable vegetation-atmosphere states to North Africa.In the early Eocene climate, the bi-stability in central Asia affects subtropical deserts on the American continents because the atmospheric circulation allows vegetation

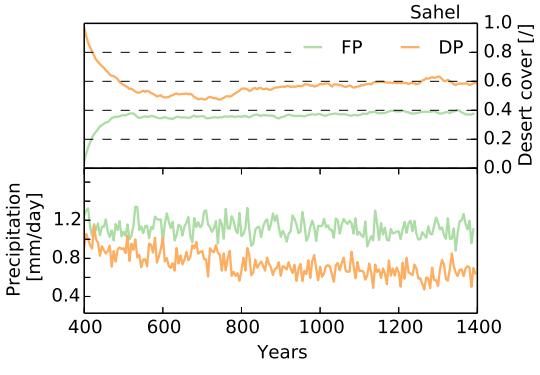

Figure 9. Time series of five-year mean desert cover and precipitation in pre-industrial Sahel in the FP_d simulation (green line) and in the DP_d simulation (orange line). The Sahel region is marked in Fig. 3.

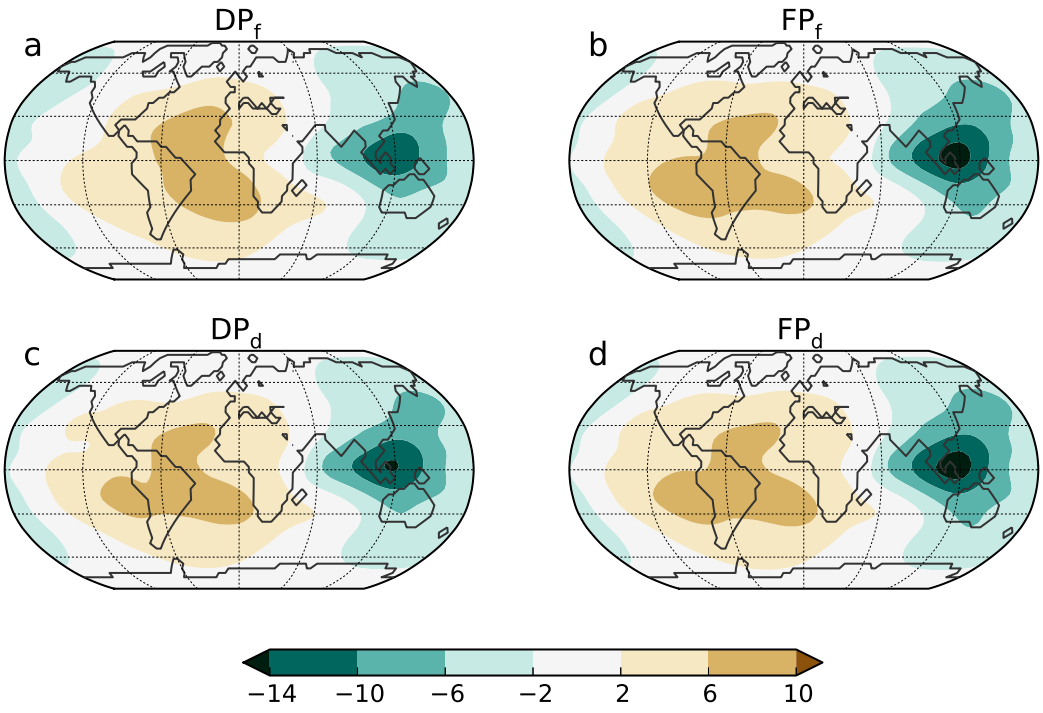

Figure 10. Velocity potential at 200 hPa at the end of the desert world simulation (a), the forest world simulation (b), the DP$_d$ simulation (c), and the FP$_d$ simulation (d). The average over the last 30 years of the respective simulation is considered. The DP$_d$ simulation and the FP$_d$ simulation start from the desert world simulation and the forest world simulation, respectively. Brown colours indicate to a positive velocity potential, upper-air convergence, and subsidence. Green colours indicate to a negative velocity potential, upper-air divergence, and rising.

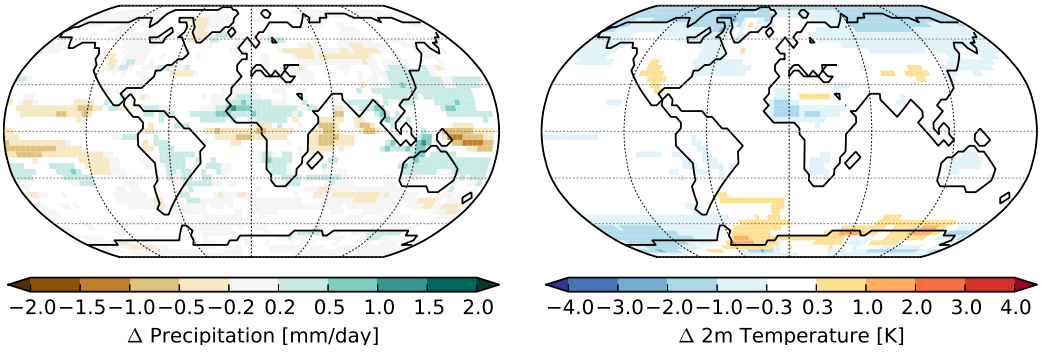

Figure 11. Differences in precipitation and 2-m temperature between the end of the FD$_P$ simulation and the end of the DD$_P$ simulation. Depicted differences are significant on a 95% level.

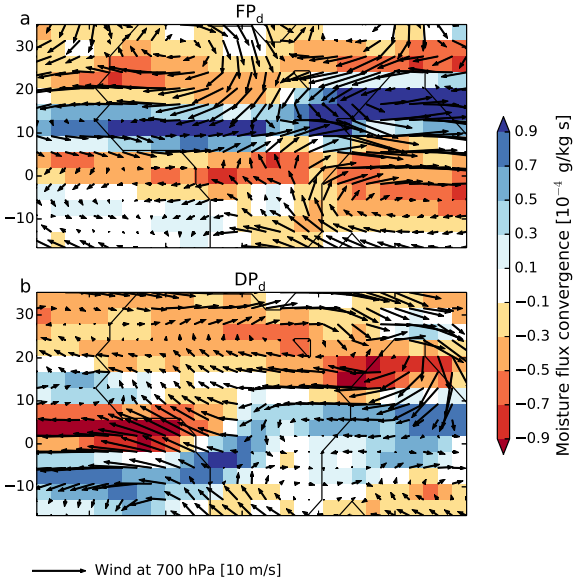

Figure 12. Horizontal wind at 700 hPa averaged over July, August, September in the last 30 years of the FP_d simulation and DE_d simulation. Shaded colors show the moisture flux convergence.

5 Conclusion

To our knowledge, the transitivity of the global climate-vegetation system has so far been explored for late Quaternary climate, i.e., glacial, interglacial mid-Holocene and present-day climate. Therefore, we extend the analysis to early Eocene conditions, i.e., to a warm, almost ice-free climate with a different configuration of continents than today. To this end, we initialise the simulations by prescribing either dense forests or bare deserts on all continents both for early Eocene and pre-industrial climate. For early Eocene conditions, multiple equilibrium states evolve: starting with desert continents, an extended desert remains in Central Asia~~to enhance the Asian monsoon and to shift global~~. Starting with complete forest cover, the Asian desert is much smaller, while coastal deserts develop in the Americas which appear to be larger than in the simulations with initially bare continents. We attribute these differences to differences in the large-scale atmospheric circulation. ~~The different stability of the vegetation-atmosphere system in the early Eocene and in the pre-industrial climateindicates that the location of the bi-stability relative to the atmospheric circulation determines the large scale extent of the bi-stability.~~

~~Time series of desert cover and precipitation in pre-industrial Sahel in the FP simulation (green line) and in the DP simulation (orange line). The Sahel region is marked in Fig. 3. Both time series show five-year mean values.~~

~~Velocity potential at 200 hPa in the DP simulation (a) and in the FP simulation (b). The average over the last 30 years of the simulations is shown. Brown colours indicate to a positive velocity~~

potential, upper-air convergence, and subsidence. Green colours indicate to a negative velocity potential, upper-air divergence, and rising.

Precipitation differences between the end of the FD_P simulation and the end of the DD_P simulation. Depicted differences are significant on a 95level. With initially forested continents, a stronger dipole in the 200 hPa velocity potential develops than in the simulation with initially bare continents. This difference prevails when vegetation is allowed to interact with climate.

As a final note, we point to the sensitivity of our results to the soil albedo. We here assume a soil albedo of 0.1 which is almost the same as the albedo of vegetation. Due to the low soil albedo, we exclude the albedo effect of vegetation and isolate the hydrological effect. Previous studies identified the albedo effect as the major driver for multiple stable vegetation-atmosphere states in the Sahel (). Other than in those studies, the bi-stabilities in our study are driven by the hydrological effect of vegetation highlighting the importance of the hydrological effectAdditional simulations with initial surface conditions that differ in the region of the Asian desert only indicate that local feedback processes are less important for the development of multiple states. When initialising a simulation with a patch of Asian desert in an otherwise completely forested world leads to mainly the same equilibrium as when the simulation is initialised with completely forested continents. The same is valid, if a patch of Asian forest is prescribed in simulations with initially bare continents. It would be interesting to find the spatial extent of the initial perturbation, or the repellor, over the Asian continent from which the system is driven into different modes.

6 Conclusion

In our early Eocene simulation, we have found multiple climate states that emerge from the intransitivity of the global climate system which are triggered by different initial conditions. These multiple states differ from those detected in similar simulations of the In the pre-industrial climateclimate, local vegetation-precipitation feedbacks seem to cause multiple equilibrium climate-vegetation states which are restricted to the Sahel region. In the simulations of the early Eocene climate, a desert in Central Asia is much larger in simulations initialised with bare continents than in simulations initialised with densely forested with large-scale initial forest cover, forests cool the Sahel in comparison with the simulations with initially bare continents. This difference results from the interdepence of vegetation and precipitation leading to a positive hydrological feedback. Most notably, the large-scale atmospheric circulation differs for the different initial vegetation covers which leads to larger coastal deserts in North and South America cooling is associated with stronger latent heat flux and stronger cloud cover. The difference in local cooling results in a stronger meridional temperature gradient between cold air above the Sahel and warmer air above the Sahara. The difference in the meridional temperature contrast, in turn, fuels the African Easterly Jet which transports moisture to the Sahel and thereby supports vegetation growth in the simulation with initially initial forested continents. Hence, in

these simulations, and in line with previous studies (e.g., Rachmayani et al., 2015), it is a local hydrological climate-vegetation feedback which leads to multiple equilibria over the Sahel region in the pre-industrial climate.

In our ~~simulations~~study, we focused on ~~the~~ biogeophysical processes and associated intransitivity of the ~~atmosphere-vegetation~~ climate-vegetation system. We neglected any differences between plant taxa and used pre-industrial plant functional types (PFTs) for the early Eocene climate simulation. ~~We assume that adjusting PFTs to early Eocene taxa will not change our results drastically even though the bi-stability in the Asian vegetation cover is associated with grasses. Grasses ocurred~~ The strongest discrepancy between Eocene plant taxa and the used PFTs concerns grasses. JSBACH considers C_3 grass and C_4, but C_3 grasses occurred rarely during the early Eocene ~~but, from the modelling point of view, grass behaves similar to herbs and fern~~ and C_4 grasses did not exist at all. To solve this discrepancy, one might exclude C_4 grasses and replace C_3 grasses by fern and herbs which grew plentifully during that time ~~(). Testing the sensitivity of our results to the used PFTs is subject to future studies.~~

~~In our pre-industrial simulations, the multiple stable vegetation-atmosphere states are predominately limited to Northern Africa. With the present-day distribution of continents, subsidence prevails over Northern Africa,~~ Utescher and Mosbrugger (2007)). Assuming fern and herbs instead of C_3 grass, we expect that fern and herbs would spread in the region where we have simulated C_3 grass before because JSBACH only distinguishes between woody vegetation, i.e. trees and shrubs, and ~~vegetation induces only weak convection thereby affects the large-scale atmospheric circulation only marginally. During the early Eocene, however, an Asian desert forms which is located in a region with large-scale upper-air divergence.In this region, vegetation induces convection and shifts large scale atmospheric circulation leading to further multiple stable vegetationstates on the American continents.~~

~~The different regional extent of multiple vegetation-atmosphere states in the early Eocene climate and in the pre-industrial climate suggest that climate and distribution of continents determines the stability of the vegetation-atmosphere system as well as the mechanisms causing multiple stable vegetation-atmosphere states. Understanding the sensitivity of multi-stabilities to constantly changing boundary contitions, such as climate and continents, deepens our knowledge about intransitive dynamcis in the climate system~~non-woody vegetation, i.e. every species except trees and shrubs. Presumably, JSBACH would handle fern and herbs in the same way as it handles grass. By allowing fern and herbs to grow in tropical temperatures, we assume that fern and shrubs would also capture the niche of C_4 grass.

Acknowledgments

We thank Veronika Gayler and Helmuth Haak (Max Planck Institute for Meteorology) for technical support~~and the anonymous reviewer their heplful comments on this~~ , and Torsten Utescher and Matthew Huber for providing the data to compare our modelling results with. The constructive critique of the anonymous reviewers, specifically the decisive question on local feedbacks in the early Eocene simulations, helped to improve our paper. This work used computational ~~recources~~ resources by Deutsches Klima Rechenzentrum (DKRZ) and was supported by the Max Planck ~~Gesellschaft~~ Society (MPG).

References

Bathiany, S., Claussen, M., , and Fraedrich, K. (2012). Implications of climate variability for the detection of multiple equilibria and for rapid transitions in the atmosphere-vegetation system. *Climate Dynamics*, 38:1775–1790.

Bathiany, S., Claussen, M., and Fraedrich, K. F. (2013a). Detecting hotspots of atmosphere-vegetation interaction via slowing down. part 1: A stochastic approach. *Earth System Dynamics*, 4:63–78.

Bathiany, S., Claussen, M., and K. Fraedrich, K. (2013b). Detecting hotspots of atmosphere-vegetation interaction via slowing down - part 2: Application to a global climate model. *Earth System Dynamics*, 4:79–93.

Beerling, D. and Royer, D. (2011). Convergent Cenozoic CO_2 history. *Nature Geoscience*, 4(7):418–420.

Bice, K. L. and Marotzke, J. (2001). Numerical evidence against reversed thermohaline circulation in the warm Paleocene/Eocene ocean. *Journal of geophysical research*, 106(C6):11529–11542.

Brovkin, V., Claussen, M., Petoukhov, V., and Ganopolski, A. (1998). On the stability of the atmosphere-vegetation system in the sahara/sahel region. *Journal of Geophysical Research: Atmospheres*, 103(D24):31613–31624.

Brovkin, V., Raddatz, T., and Reick, C. H. (2009). Global biogeophysical interactions between forest and climate. *Geophysical Research Letters*, 36:L07405.

Cerling, T., Wang, Y., and Quade, J. (1993). Expansion of C4 ecosystems as an indicator of global ecological change in the late Miocene. *Nature*, 361(6410):344–345.

Charney, J., Quirk, W., Chow, S., and Kornfield, J. (1977). Comparative-study of effects of albedo change on drought in semi-arid regions. *Journal of the Atmospheric Sciences*, 34(9):1366–1385.

Charney, J. G. (1975). Dynamics of deserts and drought in Sahel. *Quarterly Journal of the Royal Meteorology Society*, 101:193–202.

Claussen, M. (1994). On coupling global biome models with climate models. *Climate Research*, 4:203–221.

Claussen, M. (1997). Modeling bio-geophysical feedback in the african and indian monsoon region. *Climate dynamics*, 13(4):247–257.

Claussen, M. (1998). On multiple solutions of the atmosphere-vegetation system in present-day climate. *Global change biology*, 4(5):549–559.

Claussen, M. and Gayler, V. (1997). The greening of the sahara during the mid-holocene: Results of an interactive atmosphere-biome model. *Global Ecology and Biogeography Letters*, 6(5):pp. 369–377.

Claussen, M., Kubatzki, C., Brovkin, V., Ganopolski, A., Hoelzmann, P., and Pachur, H.-J. (1999). Simulation of an abrupt change in saharan vegetation in the mid-holocene. *Geophysical Research Letters*, 26(14):2037–2040.

Dekker, S. C., de Boer, H. J., Brovkin, V., Fraedrich, K., and Wassen, M. J. (2010). Biogeophysical feedbacks trigger shifts in the modelled vegetation-atmosphere system at multiple scales. *Biogeosciences*, 7(4):1237–1245.

Eberle, J. J. and Greenwood, D. R. (2012). Life at the top of the greenhouse eocene world-a review of the eocene flora and vertebrate fauna from canada's high arctic. *GEOLOGICAL SOCIETY OF AMERICA BULLETIN*, 124(1-2):3–23.

Harrington, G. J., Eberle, J., Le-Page, B. A., Dawson, M., and Hutchison, J. H. (2012). Arctic plant diversity in the early eocene greenhouse. *PROCEEDINGS OF THE ROYAL SOCIETY B-BIOLOGICAL SCIENCES*, 279(1733):1515–1521.

Heinemann, M., Jungclaus, J. H., and Marotzke, J. (2009). Warm Paleocene/Eocene climate as simulated in ECHAM5/MPI-OM. *Climate of the Past*, 5:785–802.

Ilyina, T., Six, K. D., Segschneider, J., Maier-Reimer, E., Li, H., and Nunez-Riboni, I. (2013). Global ocean biogeochemistry model HAMOCC: Model architecture and performance as component of the MPI-Earth System Model in different CMIP5 experimental realizations. *Journal of Advances in Modeling Earth Systems*, 5:287–315.

Janis, C. M. (1993). Tertiary mammal evolution in the context of changing climates, vegetation, and tectonic events. *Annual review of ecology and systematics*, 24:467–500.

Jungclaus, J. H., Fischer, N., Haak, H., Lohmann, K., Marotzke, J., Matei, D., Mikolajewicz, U., Notz, D., and von Storch, J. S. (2013). Characteristics of the ocean simulations in the Max Planck Institute Ocean Model (MPIOM) the ocean component of the MPI-Earth system model. *Journal of Advances in Modeling Earth Systems*, 5(2):422–446.

Kubatzki, C. and Claussen, M. (1998). Simulation of the global bio-geophysical interactions during the last glacial maximum. *Climate dynamics*, 14(7-8):461–471.

Lorenz, E. (1968). Climatic determinism. *Meteor. Monogr.*, 8:1–3.

Oyama, M. D. and Nobre, C. A. (2003). A new climate-vegetation equilibrium state for tropical south america. *Geophysical research letters*, 30(23):2199.

Pearson, P., van Dongen, B., Nicholas, C., Pancost, R., and Schouten, S. (2007). Stable warm tropical climate through the eocene epoch. *Geology*, 35(3):211–214.

Port, U., Claussen, M., and Brovkin, V. (2015). Radiative forcing by forest and subsequent feedbacks in the early eocene climate. *Climate of the Past Discussion*, 11:997–1029.

Pross, J., Contreras, L., Bijl, P. K., Greenwood, D. R., Bohaty, S. M., Schouten, S., Bendle, J. A., Rhl, U., Tauxe, L., Ian Raine, J., Huck, C. E., van de Flierdt, T., Jamieson, S. S. R., Stickley, C. E., van de Schootbrugge, B., Escutia, C., Brinkhuis, H., and Program, I. O. D. (2012). Persistent near-tropical warmth on the antarctic continent during the early eocene epoch. *Nature*, 488:73–77.

Rachmayani, R., Prange, M., and Schulz, M. (2015). North african vegetation-precipitation feedback in early and mid-holocene climate simulations with ccsm3-dgvm. *Climate of the Past*, 11:175–185.

Reick, C. H., Raddatz, T., Brovkin, V., and Gayler, V. (2013). Representation of natural and anthropogenic land cover change in MPI-ESM. *Journal of Advances in Modeling Earth Systems*, 5(3):459–482.

Renssen, H., Goosse, H., and Fichefet, T. (2003). On the non-linear response of the ocean thermohaline circulation to global deforestation. *Geophysical Research Letter*, 30:1061.

Stevens, B., Giorgetta, M., Esch, M., Mauritsen, T., Crueger, T., Rast, S., Salzmann, M., Schmidt, H., Bader, J., Block, K., Brokopf, R., Fast, I., Kinne, S., Kornblueh, L., Lohmann, U., Pincus, R., Reichler, T., and Roeckner, E. (2013). Atmospheric component of the MPI-M Earth System Model: ECHAM6. *Journal of Advances in Modeling Earth Systems*, 5(2):146–172.

Utescher, T. and Mosbrugger, V. (2007). Eocene vegetation patterns reconstructed from plant diversity - A global perspective. *Palaeogeography Palaeoclimatology Palaeoecology*, 247(3-4):243–271.

Wang, G. and Eltahir, E. (2000). Biosphere-atmosphere interactions over West Africa. II: Multiple climate equilibria. *Quarterly journal of the Royal Meteorological Society*, 126(565):1261–1280.

Willis, K. and McElwain, J. (2002). *The elvolution of plants*. Oxford University Press, U.S.A.

Wolfe, J. (1985). Distribution of major vegetation types during the Tertiary. *In: Sundquist E.T., Broecker W.S. (eds) The carbon cycle and atmospheric CO_2: natural variations Archean to present. American Geophysical Union, Washington/DC*, pages 357–375.

Zachos, J., Berza, J., and Wise, S. (1992). Early Oligocene ice-sheet expansion on Antarctica - Stable isotope and sedimentological evidence from Kerguelen Plateau southern Indian-Ocean. *Geology*, 20(6):569–573.

Zachos, J., Pagani, M., Sloan, L., Thomas, E., and Billups, K. (2001). Trends, rhythms, and aberrations in global climate 65 Ma to present. *Science*, 292(5517):686–693.

Zeng, N. and Neelin, D. J. (2000). The role of vegetation-climate interaction and interannual variability in shaping the african savanna. *Journal of Climate*, 13(15):2665–2670.

Table 1. List of Plant Functional Types (PFTs) defined in the land surface scheme JSBACH.

Plant Functional Type
Tropical evergreen trees
Tropical deciduous trees
Extra-tropical evergreen trees
Extra-tropical deciduous trees
Raingreen shrubs
Cold shrubs
C_3 grass
C_4 grass

Table 2. Boundary conditions in the early Eocene climate simulations and in the pre-industrial climate simulations.

	Pre-industrial	Early Eocene
CO_2 concentration	280 ppm	560 ppm
Methane	0.8 ppm	0.8 ppm
Nitrous oxide	0.288 ppm	0.288 ppm
Orbit	pre-industrial	pre-industrial
Bathymetry and orography	present-day	Bice and Marotzke (2001)
Ice sheets	pre-industrial	none

Table 3. Simulations included in the experiment.~~The same set of simulations is performed for the early Eocene climate and for the pre-industrial climate. For both climates, the simulations differ concerning the initial vegetation-atmosphere state. The simulations start either from the forest world or from the dark desert world simulated by . Soils have a homogeneous soil albedo of 0.1.~~

	Initial state	Boundary conditions
FP_d	**F**orest world	**P**re-industrial
DP_d	**D**esert world	**P**re-industrial
FE_d	**F**orest world	**E**arly Eocene
DE_d	**D**esert world	**E**arly Eocene
DA_d	Forest world with **d**esert in **A**sia	Early Eocene
FA_d	Desert world with **f**orest in **A**sia	Early Eocene